QUANTUM CHEMICAL AND SPECTROSCOPIC STUDIES OF CLOTRIMAZOLE AND RESORCINOL

BY

ABDULMUJEEB TOLUWASE ONAWOLE

A Thesis Presented to the
DEANSHIP OF GRADUATE STUDIES

KING FAHD UNIVERSITY OF PETROLEUM & MINERALS

DHAHRAN, SAUDI ARABIA

In Partial Fulfillment of the
Requirements for the Degree of

MASTER OF SCIENCE

In

CHEMISTRY

MAY, 2017

KING FAHD UNIVERSITY OF PETROLEUM & MINERALS

DHAHRAN- 31261, SAUDI ARABIA

DEANSHIP OF GRADUATE STUDIES

This thesis, written by ABDULMUJEEB TOLUWASE ONAWOLE under the direction his thesis advisor and approved by his thesis committee, has been presented and accepted by the Dean of Graduate Studies, in partial fulfillment of the requirements for the degree of **MASTER OF SCIENCE IN CHEMISTRY.**

Dr. Abdulaziz Al-Saadi
(Advisor)

24/7/2017

Dr. Abdulaziz Al-Saadi
Department Chairman

Dr. Nisar Ullah
(Co-Advisor)

Dr. Salam A. Zummo
Dean of Graduate Studies

Dr. Tawfik Saleh
(Member)

24/8/17

Date

Dr. Sulayman A. Oladepo
(Member)

Dr. M.R.S.A. Janjua
(Member)

Dedication

To my family, for their sacrifice

ACKNOWLEDGMENTS

All praise belongs to Allah, lord of all that exists and then to my advisor, Dr. Abdulaziz Al-Saadi, my committee members; Dr. Nisar Ullah, Dr. Tawfik Saleh, Dr. M.R.S.A. Janjua and Dr. Sulayman Oladepo. I appreciate the support of the faculty and staff of Chemistry department especially Dr. Abulkibash, Dr. Chanbasha and Dr. Al-Hooshani. Also, I would like to appreciate Dr. Abdullah Sultan, Dr. Safwat Abdelazeim and Dr. Alexis Nzila. I am most grateful to the members of the Nigerian community in KFUPM for their help in several ways particularly; Mr. Kazeem Sulaiman, Dr. Saheed Popoola, Dr. Saheed Adekunle, Mr. Nasirudeen Ogunlakin, Mr. Cheche Abubakar; who doubled as my room and class mate, Mr. Isaiah Adelabu, Mr. Ismail Yunus, and Mr. Kabiru Haruna. I would also like to appreciate my friends from other nationalities particularly Dr. Adam Seliman, Mr. Faisal Alrasheed and Mr. Mutasem Al-Shalalfeh. My appreciation would be incomplete without appreciating the sacrifice of my family, most especially my wife, Rukayat and my son, Abdus-Samad; and to my siblings and parents for taking care of them during my absence. I pray and hope the sacrifice would be worth it.

TABLE OF CONTENTS

LIST OF TABLES

LIST OF FIGURES

LIST OF ABBREVIATIONS

CADD	:	Computer-Aided Drug Design
DFT	:	Density Functional Theory
PDB	:	Protein Data Bank
FMO	:	Frontier Molecular Orbital
HOMO	:	Highest Occupied Molecular Orbital
LUMO	:	Lowest Unoccupied Molecular Orbital
MEP	:	Molecular Electrostatic Potential
PES	:	Potential Energy Surface
FT-IR	:	Fourier Transform Infra-Red
CTZ	:	Clotrimazole
MTZ	:	Methimazole
KTZ	:	Ketoconazole
SAP	:	Secreted Aspartic Proteinase
HS	:	Hidradenitis Suppurativa
MNPE	:	(4-(3-methoxy-4-nitrophenyl)piperazin-1-yl)ethanone

ABSTRACT

Full Name : Abdulmujeeb Toluwase Onawole

Thesis Title : Quantum chemical and spectroscopic studies of clotrimazole and resorcinol

Major Field : Chemistry

Date of Degree : May, 2017

Bioactive compounds such as clotrimazole and resorcinol are important antimicrobial agents. Clotrimazole is effective against Candidiasis while Resorcinol is used in treating acne. Quantum chemical studies such as Density Functional Theory (DFT) and molecular docking are important tools in understanding the molecular properties of bioactive compounds most especially the mode of action by which they act as drugs. Understanding these properties would help in future drug development especially now that most microbes are developing resistance to already approved drugs. Computational analysis and spectroscopic characterizations of clotrimazole, resorcinol, resorcinol -OD isotopomer, and resorcinol dianion salt were investigated. Infrared and Raman spectroscopic techniques were used for the structural characterization. Conformational analysis using potential energy surface scans via DFT was done for both clotrimazole and resorcinol. The energetically minimized forms and vibrational spectra were computed using ab initio and DFT quantum chemical techniques utilizing 6-311++G(d,p) basis sets. The unit cell of the room-temperature stable α-resorcinol and its –OD isotopomer were optimized at the B3LYP/6-311+G (d,p) level of theory and was shown to adopt a near Cs symmetry. Assignments of local vibrational modes associated with the crystal structure were also carried out. Relative stability analysis from the MP4 level, the syn-syn (S) form of resorcinol is predicted to be about 0.8 kcal/mol higher in energy than the most stable anti-syn (AS) form. The out-of-plane vibrational modes of the solid sample exhibit some spectral shifts as compared to the gaseous phase as a result of the strong intermolecular packing forces. Molecular docking study exhibited that resorcinol is keratolytic active and

tends to form a stable complex in its near-AS form with Keratin-7. The conformational analysis of clotrimazole gave rise to three possible conformers. The geometrical parameters calculated at (B3LYP/6-311++G(d,p)) of the clotrimazole were in agreement with the XRD results. The calculated FMO energies gave insight into the molecular properties which disclosed that charge transfer occurs in the molecule and showed that the HOMO occurred on the imidazole ring while the LUMO occurred on the benzene rings. The MEP map showed that the negative region is localized in the imidazole ring and hence prone to electrophilic attack. The protein-ligand interaction of the title compound with Secreted Aspartic Proteinase 2 of C. albicans using molecular docking studies gave insight into its mode of action in treating Candidiasis.

ملخص الرسالة

الاسم الكامل: **عبدالمجيب تلويس أوناوول**

عنوان الرسالة: **دراسة التحليل الطيفى وكيمياء الكم لمركبات كلوترايمازول والريسورسنيول**

التخصص: **علوم الكيمياء**

تاريخ الدرجة العلمية: مايو 2017

الكلوترايمازول والريسورسينول هما من المركبات ذات الفاعلية الحيوية التي تلعب دوراُ مهما كعوامل متضادة للميكروبات. الكلوترايمازول فعال ضد فطريات الجلد بينما الريسورسينول تكمن فعاليته في معالجة حب الشباب. وتعتبر دراسات كيمياء الكم مثل نظرية الكثافة الوظيفية ونظرية الإلتحام الجزيئية كأدوات مهمة لمعرفة الخصائص الجزيئية لهذه المركبات ذات الفعالية الحيوية وبالأحرى معرفة طريقة عملها كأدوية. معرفة خصائص هذه المركبات قد تمكن في المستقبل من تطوير الادوية خصوصا مع تطوير الميكروبات لمقاومتها ضد الأدوية المسموح بها حاليا. تم تشخيص مركبات الكلوترايمازول والريسورسينول والريسورسينول المتناظر بالأضافة إلى الريسورسينول ثنائى الملح بواسطة التحليل المحوسب والتوصيف الطيفى. وكذلك أستخدمت تقنية مطيافية الأشعة تحت الحمراء ومطيافية رامان في التوصيف التركيبى لهذه المركبات. تحليل التكوين الجزيئى للكلوترايمازول والريسورسينول أجرى بماسح طاقة السطح الموضعية بأستخدام نظرية الكثافة الوظيفية. الأطياف الأهتزازية والانماط المخترلة بالطاقة حوسبت بواسطة تقنيات نظرية الكثافة الوظيفية وابانيشو بأستخدام

6- 311++G(d,p) basis sets.

وحدة الخلية المثلي لاستقرار الريسورسينول والريسورسينول المتماثل فى درجة حرارة الغرفة تم ضبطها بواسطة B3LYP/6-311+G (d,p) level of theory والتي تتخذ عرض ذرات الكربون المتماثلة القريبة

كما تم تحديد أنماط الأهتزازات المحلية المرتبطه بالشكل البلورى. تحليل الاستقرارية النسبية من مستوى MP4 and the syn-syn (S) form و للريسورسينول قدر بحواالى 0.8 كيلو سعر لكل مول له طاقة أكثر من

the most stable anti-syn (AS) form.

أنماط الاهتزازات خارج السطح للعينة الصلبة أوضحت تغيرات طيفية مقارنة بالحالة الصلبة نتيجة لقوة الجزيئات البينية لقوي التعبئة. دراسة إلتحام الجزيئات أوضحت ان الريسورسينول نشط للقرنية وله ميل لتكوين مركب مستقر فى متشاكله اي اس مع الكيراتين-7.

تحليل التكوين الجزيئ للكلوترايمازول اعطي ثلاثة متشاكلات محتملة. تم حساب عوامل الشكل الهندسى على قاعدة

(B3LYP/6-311++G(d,p))

للكلوترايمازول والتى لها توافق مع نتائج حيود الاشعة السينية. طاقات اوربتالات جزيئات فيرمى المحسوبة بالنسبة للخصائص الجزيئية أوضحت حدوث إنتقال الشحنة فى الجزيئ وبناءً عليها فإن الاوربتالات الجزيئية الممتلئة العليا تحدث علي حلقة الاميدازول بينما الاوربتالات الجزيئية الفارغة الدنيا تحدث علي حلقات البنزين. أوضحت خريطة ام اي بي إن المنطقة السالبة تقع على حلقة الاميدازول نتيجة للهجوم الالكتروفيلى. تفاعل البروتين- اللاقطة بالنسبة للمركبات موضوع الدراسة مع أسبارتك بروتينيز-2 المستخلص من سى ألبيكان بإستخدام دراسات إلتحام الجزيئات اعطى نظرة فاحصة لطريقة عمل هذه المركبات لعلاج فطريات الجلد.

CHAPTER 1

INTRODUCTION

Antimicrobial agents which are compounds that destroys microorganisms including fungi, bacteria and other microbes are often classified based on the microorganism they act upon. Clotrimazole acts on the fungus *Candida albican*s which is the pathogen for candidiasis[1] and hence it is called an antifungal while Resorcinol is active against *Propionibacterium acnes* the bacterium that causes hidradenitis suppurativa (acne)[2], [3] hence, it is an antibacterial drug. Quantum chemical studies which includes Density Functional Theory (DFT) and Molecular docking have been widely used in studying bioactive compounds and classified under *in silico* methods [4] in drug discovery which is literally means in silicon referring to the silicon chips in computers.

Designing drugs used to be a very expensive and cumbersome process. However, the advent of Computational Chemistry has proved a very useful tool in Medicinal Chemistry and in understanding the mechanisms by which drugs function. This information is important because it helps in the designing of new drugs [5]. Also Computer-Aided Drug Designing (CADD) has helped in reducing the cost in both time and money of drug development [6] Stereochemical behavior often influences the physicochemical properties of a compound [7]. For bioactive compounds, they have a particular influence on a molecule's ability to interact with a protein target. Molecular docking involves predicting the most preferred conformation or orientation of a small molecule (bioactive compound)

when it bounds to a large molecule (protein). The way the small molecular binds to the protein can help predict the binding affinity and also the mode of action of that small molecule. Spectroscopy is also an important tool in drug design especially when it comes to characterization during drug delivery and drug formulation [8]. This is very important in how a drug is absorbed in the body. DFT complement the experimental spectra in assigning vibrational bands so as to distinguish the different functional groups present in bioactive compounds. Upon the application of molecular docking in understanding the mode of action of resorcinol and clotrimazole which are approved drugs. Molecular docking was applied in methimazole and ketoconazole and also newly synthesized piperazine and inorganic complex compounds which showed promise as anti-stress and anticancer agents respectively.

1.1 Clotrimazole

Clotrimazole (CTZ), 1-[(2-Chlorophenyl)(diphenyl)methyl]-1H-imidazole is a derivative of imidazole and is being used to treat fungal or yeast infections that affects the skin areas such as the feet (Athlete's foot) and even the vagina. It is mainly used to treat candidiasis, a fungal disease, which is caused by the pathogen *Candida albicans (C. albicans).* CTZ is applied as a cream on the affected areas of the skin or it is taken orally in tablet form. It is presumed that it inhibits the proteins in the fungal cell membrane which leads to the permeability of the membrane and ostensible disturbance of the enzymes bound to the membrane [9], [10]. *C. albicans* is an important agent of infection, which engages in a parasitic relationship with its host especially when the hosts have deficient immune system such as HIV/AIDS (Human Immuno-deficiency Virus/Acquired Immuno-deficiency Syndrome). Several studies have been directed on understanding the cell surface of *C.*

albicans mainly because of the two main functions of the cell surface which includes maintenance of the shape of the fungus acting as a permeable membrane and secondly, the interaction of the fungi with its external environment which include its host [11]. The latter part of the function of the cell surface highlights the reason why most research is on the cell surface of C. albicans. Candida albicans is the most common strain of Candida which is the pathogen for Candidiasis [12]. Over 150 species of Candida exist some of which include *C. tropicalis, C. krusei* and *C. glabrata.* Candida can be found in all humans. Their cell walls are thin and they are about 6 microns in length. They actually exhibit a commensal relationship in humans [13]. However, when they reproduction is in excess they become parasitic. The presence of virulent secreted aspartic proteases (SAPs) and other metabolites lead to a disruption in the energy cycle and hence fatigue in the host. Curd-like discharge from the vagina and white patches in the tongue area are a few symptoms of Candidiasis [14]. Anti-fungal agents such as CTZ and other Imidazole related compounds like fluconazole and ketoconazole are used in treating Candidiasis [15]. CTZ has been known to display its antimycotic activity by inhibiting the fungi cytochrome p450 14α-lanosterol-demethylase (14-LD) commonly referred to as CYP51 [16]. This is done by restraining the biosynthesis of the sterol in particular the sterol auxotrophic strain including the demethylase [17]. This makes the membrane permeable and leads to a disruption between the enzymes and the membrane it bounds on. This action of CTZ prevents the further division and growth of *C. albicans*. However, there are speculations that CTZ may also interact with phospholipids and other proteins in the cell membrane of *C. albicans* [10]. Bilensoy et al [18] and Robbe et al [19] reported the experimentally observed IR and Raman spectra of CTZ respectively while Dhudashi et al [20] used HPLC

method to estimate the CTZ in lotion and cream dosage form. Song and Shin [1] reported the XRD crystal structure of the title compound. In this present work, the conformational analysis, molecular and spectroscopic properties including vibrational assignments have been reported which to the best of our knowledge has not been done till date. Molecular docking studies of CTZ with a virulent protein present in *C. albicans* using the possible conformations was also reported to give insight into the possible mode of action of CTZ in the cell membrane of *C. albicans*

1.2 Resorcinol

Resorcinol (1,3-dihydroxybenzene) is a fundamental organic compound that finds several applications in pure and applied fields of science [6,7]. Because of its pharmacological and biological importance, especially as a potent antibacterial agent [1], resorcinol remained a subject of extensive studies for its electronic ground and excited states from experimental and theoretical points of view. Resorcinol is a simple chemical compound that has been in use for more than a century. Nevertheless, it is not widely known despite its many applications except among non-specialist in the field of resorcinol chemistry [21], [22]. Resorcinol is a white crystalline solid which often exist in both α and β form which are both formed by the crystallization of resorcinol from ethanol and benzene respectively [21]. Resorcinol is a relatively less toxic compound compared to phenol [23]. Hence, its use in the pharmaceutical industry. It can easily be absorbed by the skin and causes irritation upon exposure to the eyes and during inhalation. However, it is stable under flammable conditions [24]. 2-methoxy resorcinol is a derivative of pyrogallol, a toxic natural product [25] mostly found in plants. However, its applications are found in supramolecular

photochemistry [26] and also has a uremic retention solute used in recognizing protein-bound compounds [27].

Halogenated resorcinols are one of the most useful derivatives in resorcinol chemistry. They are formed via electrophilic aromatic substitution with the respective halogen atom. The presence of two hydroxyl groups cause higher activation, which consequently allows easy halogenation of resorcinol at the 2, 4 and 6 positions. Fluoro resorcinols are used in dye preparation, particularly fluorescein and rhodol dyes, 2-chloro resorcinol is a precursor in preparing 1,2-benzisoxazoloxy acetic acids, which is an antihypertensive drug while 4-chloro resorcinol is used in preparing photoactive compounds which are applied in photolithography. Brominated and iodinated resorcinol compounds are used to alleviate the impact caused by fires and in radiology diagnosis respectively [22].

During the past decades resorcinol exhibited a number of medical applications, especially as it is used as a starting material to prodcue derivatives of Active Pharmaceutical Ingredients (API) for treating Alzheimer's disease, sickle cell anemia and alcoholism [22]. However, resorcinol itself has been also used as a topical agent in treating dermatological diseases such as eczema, acne and Hidradenitis Suppurativa (HS) [29,30]. Molecular docking is a useful tool used in structure-based drug design (SBDD) to predict binding affinities of an API with specific protein targets [30] that play a role in the pathology of a disease. Resorcinol possess keratolytic properties and hence is known to target the follicular keratin plug which is the initiation stage of several HS lesions [29]. Therefore, a molecular docking analysis is useful to provide insights on the modes of action of resorcinol in treating HS.

CHAPTER 2

LITERATURE REVIEW

2.1 Clotrimazole

Candida albicans is one of the popular fungal pathogens responsible for causing Candidiasis. It engages in a parasitic relationship with its host even though it initially engages in a commensal relationship[11], [31]–[33]. This parasitic relationship is often worse when it occurs in that hosts have deficient immune systems, such as HIV/AIDS because they have T-cell deficiencies[11]. Though it is still unclear in mycology how the relationship changes from commensal to parasitic[31]. Candidiasis also particularly affects about 75% of the women population experience candidiasis in the form vulvovaginal candidiasis[34]. C.albicans are also known to play a role in early childhood caries which is the presence of decayed cavities in a child of equal or less than 6 years of age [35]. Other fungal pathogens aside *C. albicans* that cause yeast infections include *C. tropicalis* and *C. glabrata.* However, *C. albicans* is the most renowned amongst them all [31]. Several studies have been directed at understanding the cell surface of *C. albicans* mainly because of the two main functions of the cell surface which include shape maintenance of the fungus and secondly, the interaction of the fungi with its external environment which include its host [11]. The latter part of the function of the cell surface highlights the reason why most research is focused on the cell surface of *C. albicans.* The virulence attributes of *C. albicans* includes phenotypic switching, dimorphism, hyphal formation and secretion of extracellular hydrolytic enzyme which includes aspartyl proteinases which are also called aspartic proteinases[36], [37].

Secreted Aspartic Proteinases (SAPs) are known to be located at the surface of the cell. They are encoded by a multigene family which is includes the presence of 10 SAP genes (SAP1-10)[38]–[42] which have been detected under many laboratory conditions[43]. Asides been among the virulence factors in Candidiasis, the activities of SAPs also contribute to tissue damage of the host, particularly SAP 1-3[44]. Removal of SAP1-6 have been suggested to assuage virulence in candidiasis keratitis [45]. Nevertheless, SAP1-10 are contributing factors when it comes to vaginal candidiasis[46], [47]. The activities of SAP depend on pH, SAP1-3 are more active in lower pH(3-5) while SAP4-6 are more active at higher pH values (5-7)[32]. Though the normal pH of blood is neutral (7.4). However, the pH values vary through the body, such as the vagina area which is more acidic and the oral cavities which is neutral. Hence, the reasons why some SAP thrive more in certain areas of the body[32]. Since, SAPs plays a major role in many stages of infection of candidiasis, this makes it a potential drug target for treating Candidiasis infections[48], [49]. Pepstatin A has been used to inhibit SAPs[11]. However, there is need for new SAP inhibitors as there are new pathogenic fungal species, antifungal resistance, drug interactions and bioavailability amongst many other factors[48].

Azole based compounds alongside, polyenes are the most popular anti-fungal drugs used in treating candida infections[50]. However, polyenes have shown to be toxic hence the decrease in their use in treating candidiasis as compared to azole based compounds which are much safer[51]. Amphotericin B (AMB) is the most popular amongst the polyenes primarily because of the low occurrence of fungal resistance against it. However, it is nephrotoxic[50]. The known mode of action of antifungal drugs is to target the cell wall or membranes of the pathogen[10]. Hence the polyenes bind to ergosterol, the major sterol

of fungal membranes while the azoles inhibit of the fungal cytochrome P450-dependent lanosterol-14-α-demethylase which consequently leads to ergosterol reduction[16], [50], [51]. This action makes the membrane permeability and consequently leads to the disruption of enzyme systems bound to the membrane[52]. However, recent studies have shown that SAPs contribution to C.albicans virulence and hence are a potential drug target[31], [44], [53]. Many azole compounds have been designed over the years to improve the treatment of candidiasis. Ketoconazole proved to have superior in vivo activity and lower degree of inactivation after being absorbed as compared to other azole antifungal drugs such as clotrimazole[54]. Ketoconazole is also the only known antifungal drug to bind to the androgen receptor[55], [56]. Fluconazole and Itraconazole are also proven to be more effective than Clotrimazole and Nystatin(a polyene) when it comes to treating oropharyngeal candidiasis[57]. However, Clotrimazole has also shown to be successful in treating vaginal candidiasis as compared to the popular polyenes (AMB and Nystatin). Nevertheless a demerit of Clotrimazole is its side effect neurological reactions and gastro-intestinal troubles[58]. Itraconazole is very active against mucosal form of candidiasis and it is quite similar to Fluconazole with respect to its activity. However, the latter has different pharmacological properties and does not violate any of the Lipinski's rule of five (RO5)[59], [60] alongside voriconazole[61], [62]. Azole based compounds have also recently been applied in corrosion inhibition[63] and Surface Enhanced Raman Spectroscopy (SERS)[64], [65].

2.2 Resorcinol

Resorcinol (1,3-dihydroxybenzene) is an important building block in organic synthesis and finds several applications in pure and applied fields of science [66], [67]. Because of

its pharmacological and biological importance, in particular its use as a potent antibacterial agent [68], resorcinol has been a subject of extensive interest both from experimental and theoretical points of view [22]. In the solid and gas phases, three possible rotamers of resorcinol are known (Scheme 1).

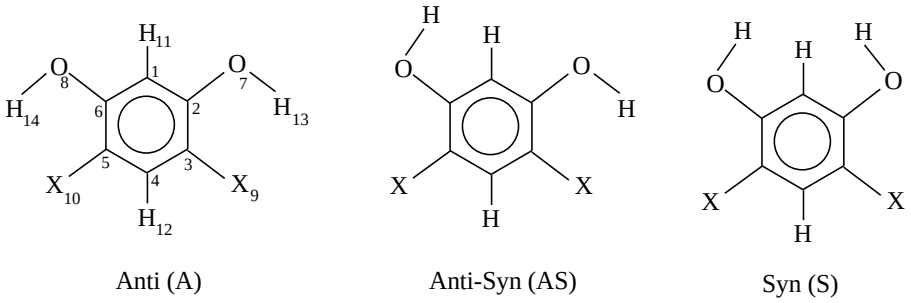

Anti (A) Anti-Syn (AS) Syn (S)

Scheme 1. Atom numbering and the three possible rotamers of resorcinol

In case of solid-phase resorcinol, intermolecular interactions are stronger, which is due to solid packing arrangement. Based on x-ray crystallographic analysis, resorcinol exists in two forms i.e., α- and β-resorcinol. The crystal structure of α-resorcinol, the stable form at the room temperature and atmospheric pressure, was first reported by Robertson [69]. The study revealed that molecules in α-resorcinol maintain the anti-configuration (**A**) of C_{2v} symmetry [69]. The crystal phase structure of α-resorcinol is stabilized by intermolecular hydrogen bonding with a distance in the order of 2.7 Å. Two years later, the crystal structure of β-resorcinol, which arose due to phase change at 347 K, was also disclosed [70]. In the case of β-resorcinol, the molecular conformation interconverts into the C_s anti-syn (**AS**) configuration. β-Resorcinol was shown to have a denser phase with a nearly 3% volume contraction [70]. In both systems (α & β-resorcinols), the unit cell contains four resorcinol molecules with different molecular packing and lattice parameters [22], [69]. Raman

spectroscopy has been used to characterize the α to β phase change and study different nature of intermolecular hydrogen bonding networking as the resorcinol changes from one crystalline phase to another [70], [71].

Moreover, studying the properties of the three possible rotamers of resorcinol in the gas phase has been of great interest. In previously reported spectroscopic studies, anti-syn (**AS**) and anti (**A**) rotamers were readily identified due to their comparable stabilities. The free-jet spectrum of resorcinol with only a single origin in the near-UV region was first disclosed in 1950 [72]. This was followed by a report by Dunn *et al* [72] on high-resolution laser resonant two-photon ionization (R2PI) spectra of resorcinol, which permitted the identification of three distinct rotamers of the compound. The resonance-enhanced multiphoton ionization (REMPI) and hole-burning (HB) spectra of resorcinol were also recorded by Gerhards *et al* [73] wherein both **AS** and **A** rotamers were identified. In 1996, Melandri *et al* [74] confirmed the coexistence of the three configurations of the compound in the gas phase by free-jet millimeter wave (MW) spectrum [75]. The study revealed that **A** and **AS** forms possess relatively similar stability whereas the **S** form lies at least 400 cm^{-1} higher in energy. The careful assignments of the vibronic states in the dispersed fluorescence (DF) spectra of resorcinol confirmed the presence of the more stable **A** and **AS** forms although there was a little variance in the spectral features between the two rotamers [76]. Moreover, the **A** and **AS** rotamers of resorcinol and its deuterated analogs in their S_0 and S_1 electronic states were also confirmed by the high-resolution UV spectroscopy [75]. However, the study did not cover investigation of the **S** rotamer. In the same study [75], automated assignments have been performed using a genetic algorithm approach with an asymmetric rotor Hamiltonian. Later, Gerhards *et al* [76] have reported the mass analyzed threshold ionization

(MATI) and infra-red photo induced Rydberg ionization (IR-PIRI) spectra of resorcinol and its cationic species wherein they observed the **A** and **AS** conformers of the compound (Claudio and Ha, 1990; Gerhards et al., 1998). Thus, it can be concluded that the **AS** and **A** forms of resorcinol are more stable in the gas phase compared to the **S** form. These findings were further supplemented by theoretical calculations together with some of the aforementioned structural and conformational spectroscopic investigations [76]–[78] Additional computational studies on the energetics and structural properties of resorcinol have also been reported [77]. The predicted energy differences between the three isomers (**AS**, **A** and **S**) of resorcinol at the HF/4-31G* level was found to be smaller (0, 84 and 378 cm^{-1}, respectively) with a rotational barrier around the C-OH bond in the order of 2-3 kcal/mol [78]. Computational studies have been extended to the crystal phase of resorcinol. The crystal morphology and solvent effect on the crystal habit of resorcinol and other organic systems by *ab initio* calculations were studied [79]. Moreover, the stability and lattice parameters of the two crystalline phases of resorcinol were explored by molecular dynamics calculations in an NPT ensemble [80], showing good agreement between the predicted properties and experimental data earlier reported. Moreover, theoretical methods have been employed to understand the nature of interaction between resorcinol and different solvents [81]–[83]. Blanco *et al* have explained the overlapping pK_a values of resorcinol determined by UV-Vis spectroscopic techniques with the help of HF and DFT-B3LYP calculations [84]. The theoretical data enabled to explore the molecular conformations and solute–solvent interactions of the resorcinate anions. Moreover, B3LYP method was employed [85] to interpret the solvation effect by predicting total energies, dipole moments, reactivity parameters and transition states involved in resorcinol-solvent species. A theoretical

resorcinol-water model of 1:2 stoichiometry was investigated to explain the high dipole moment (8.6 D) of resorcinol in water [85].

The assignments of the vibrational modes of resorcinol in crystal and gaseous phases by a number of spectroscopic techniques were also carried out, which provided deeper understanding of the electronic and rotameric nature of resorcinol. The vibrational assignments based on its infrared and Raman spectra in the solid phase were first reported by Penot *et al* [81] and Hidalgo *et al* [82]. Later on, a number of these assignments were revised by Green *et al* [83]. The gas-phase infrared spectrum of resorcinol in the range 4000-625 cm^{-1} at 190°C was recorded by Wilson [86]. Detailed assignments of the IR bands revealed that the single molecule adopts a C_s symmetry structure that corresponds to the **AS** rotamer. In a recent gas-phase study [87], the analysis of the vibrational states by the dispersed fluorescence (DF) spectrum of resorcinol in the free jet revealed the coexistence of **AS** and **A** rotamers. Moreover, the polarized infrared spectrum of α-resorcinol crystals in the lattice mode and internal vibration regions at lower temperatures have been reported [88]. Particularly, O-H stretching frequencies have been investigated by means of infrared photo induced Rydberg ionization (IR-PIRI) [89] and non-resonant ionization detected (NID) infrared and near-infrared (IR-NIR) spectroscopic techniques [78]. The assignments of the ν_{OH} stretching overtones of resorcinol clearly confirmed the existence of the two nonequivalent O-H bonds associated with the **AS** rotamer. In addition, the other two rotamers could also be assigned in the overtone spectra with the help of harmonic oscillator local mode calculations performed at the B3LYP/6-311++G(3df,2pd) level [89].

Herein, we wish to report our study based on extensive vibrational frequency calculations based on both the single molecule and unit-cell system of crystalline resorcinol. The infrared, Raman and ^{1}H NMR analyses of resorcinol-OD and resorcinol dianion salt have also been performed and compared with the resorcinol. The conformation of resorcinol has been explored at different calculation levels for a more accurate energetic description and to achieve reliable understanding of the molecular docking mechanism towards keratin-7.

CHAPTER 3

METHODOLOGY

3.1 Experimental Details

The studied of clotrimazole and resorcinol were purchased from Sigma Aldrich and used without any additional refinement for spectroscopic analyses. The mid-infrared spectra (4000-400 cm^{-1}) were collected at room temperature using a Nicolet 6700 FT-IR spectrometer equipped with a globar source, a KBr beam splitter, and a DTGS KBr detector at one-wavenumber resolution using a KBr window. The Nicolet 6700NXR FT-Raman module equipped with a CaF2 beam-splitter and an InGaAs detector was used to collect the Raman spectra (4000-100 cm^{-1}) of the three compounds at room temperature. The He-Ne laser source operating at 1064nm with 0.2 W was used for sample excitation.

3.2 Computational Details

All the computational calculations of the studied molecules were done with the Gaussian 09 program [90] using the Density Functional Theory. The molecules were optimized at the B3LYP method using the 6-311++G(d,p) as the basis set. The vibrational frequencies were calculated for all the studied molecules and no imaginary frequencies were present. The VEDA program [91] alongside GaussView [92] were used to assign the vibrations of all the molecules. The frequencies calculated were scaled to have a reasonable comparison with the experimentally determined ones using the method developed by Saadi and Laane [93]. Frequencies within the range of 2700 cm-1 and 4000 cm-1 used a scaling factor of 0.961 while those within the range of 0 to 1800 cm-1 used 0.985 as the scaling factor. The proteins structures were downloaded from the protein data bank (PDB) [94] and were

validates using Ramachandran plots via the Moleman 2 program [95]. All the molecular docking studies were calculates using the CLC drug discovery workbench 3.0.2 [96]and the molecular interactions were viewed using Discovery studio [97].

CHAPTER 4

RESULTS AND CONCLUSION

4.1 Clotrimazole

4.1.1 Molecular structure

CTZ is a non-planar compound that contains 4 ring structures which include two benzene rings, a chlorobenzene and an imidazole ring. The four rings are connected by a quaternary carbon at the center as seen in Fig.1 which gave the structure a C_1 symmetry point group. Song and Shin [1] had described the crystal structure of CTZ. The Potential Energy Surface (PES) Scans depicted in Figs 5 and 6 showed rotations around the C_6-C_7 and C_7-N_{10} bonds respectively. The PES resulted in four energy conformations; A B and C (Fig. 2). It was observed that CTZ had low stability whenever the chlorine atom was close to any of the aromatic rings as seen in conformers A and C (Figs. 3 and 4). This might be due to steric crowding which also involves the repulsion between the negative electrons of the chlorine atom and the pi-electrons present in the aromatic rings and hence the most stable structure conformation occurred when the rings where most far apart (conformer B) to minimize repulsion. The energy difference between the most stable conformer and the least unstable conformers is about 5kcal/mol. In the first PES scan (Fig. 3) which has C_6-C_7 has its rotational bond, it was observed that the chlorobenzene moved about 180° from conformers A to B. The relative energy difference was about 5kcal/mol though the energy. However, in the second PES scan (Fig. 4) which has its rotational bond at C_7-N_{10}, it was observed that a 180° flip in the imidazole ring from conformer A led to a lower energy conformer C which had a relative energy difference of less than 1kcal/mol. The PES was also carried out in aqueous phase and

the results showed the same conformations as in gas phase except that the energies were slightly higher (Table 1). Hence, CTZ is less stable in aqueous phase than in gas phase. The PES revealed Conformer B has the most stable while conformer A and C had similar stabilities. Conformer B's stability is due to the absence of steric crowding and repulsive effect between the chlorine atom and the benzene ring.

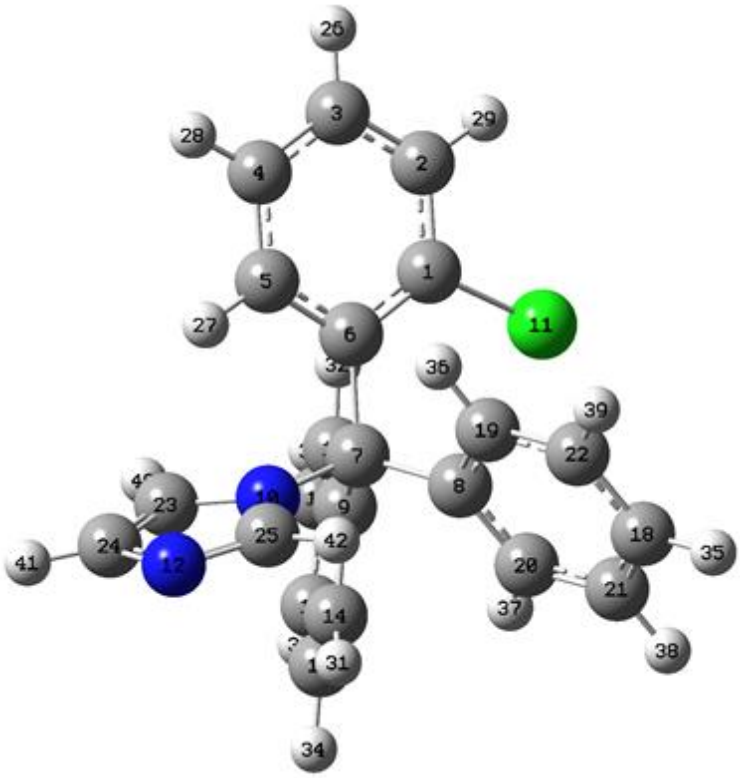

Figure 1. The optimized geometry (DFT) of CTZ

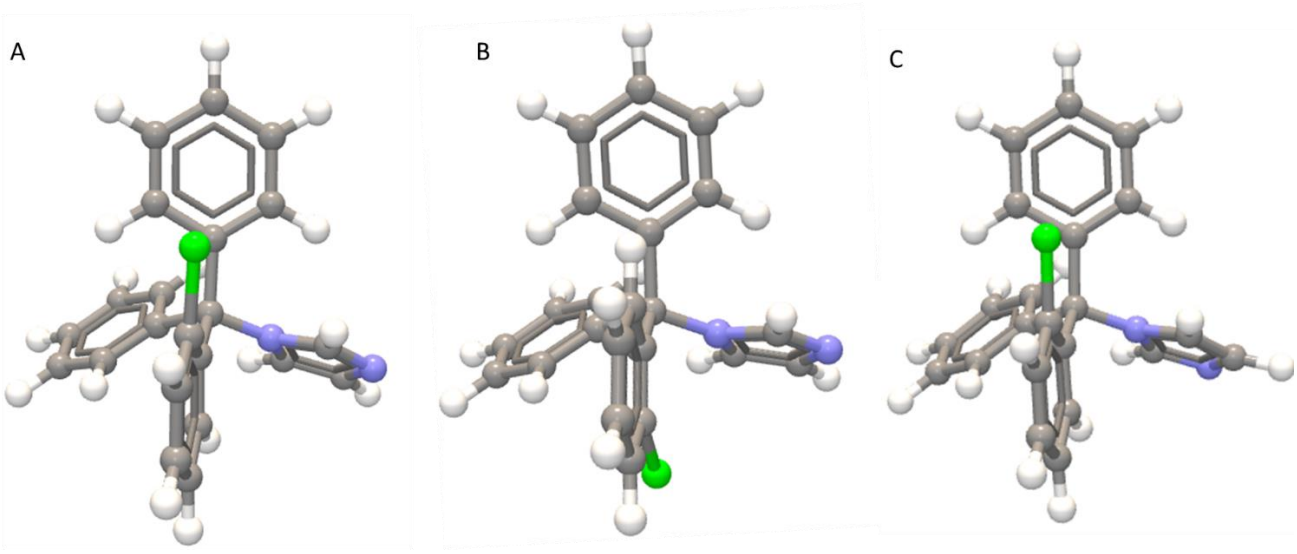

Figure 2. The three possible minimal energy conformations of CTZ

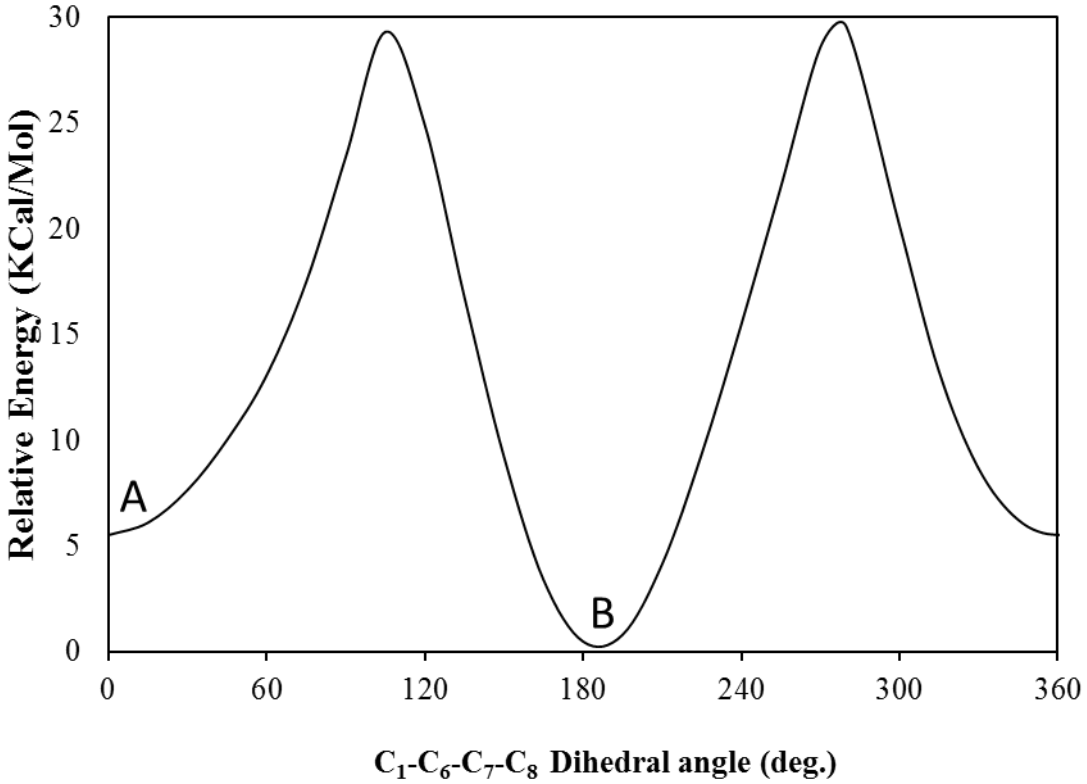

Figure 3. Potential energy scan resulting from the rotation about the C_1–C_6–C_7–N_{10} bond as calculated at the B3LYP/6-311++G (d,p) level of theory.

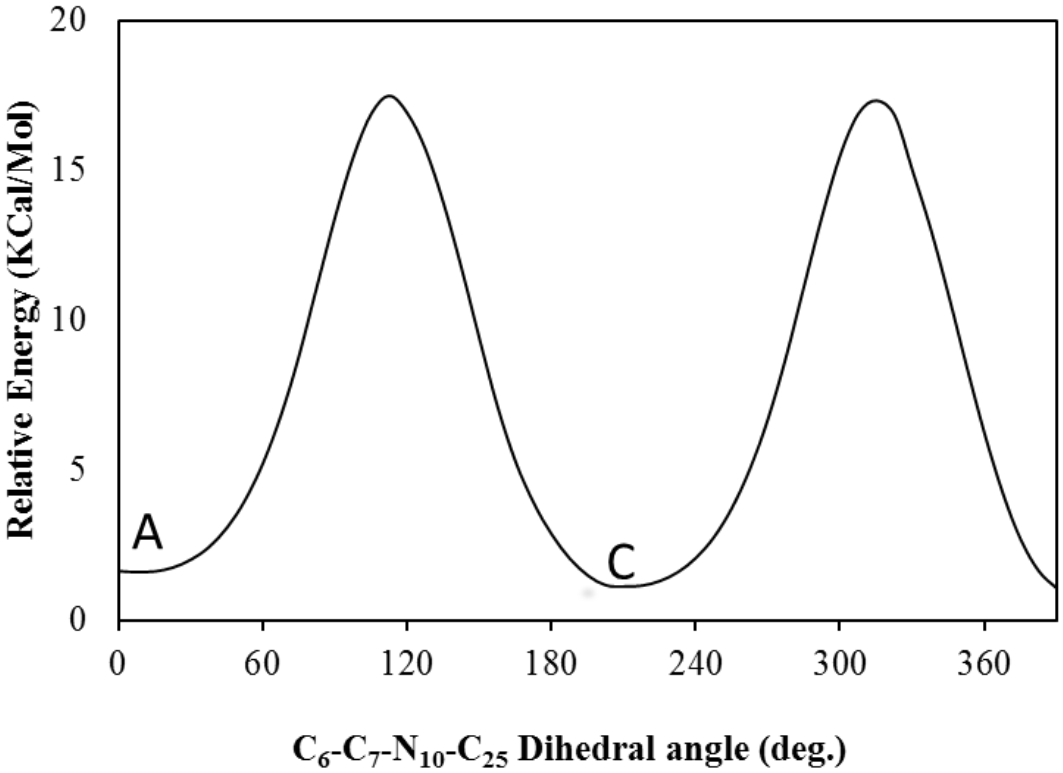

Figure 4. Potential energy scan resulting from the rotation about the C_6–C_7–N_{10}-C_{25} bond as calculated at the B3LYP/6-311++G(d,p) level of theory.

Table 1. The relative energies from the three possible conformers of clotrimazole in gas and aqueous phases.

Conformers	Gas phase (kcal/mol)	Aqueous phase (Kcal/mol)
A	5.195	5.265
B	0.000	0.000
C	4.808	4.958

4.1.2 Geometrical parameters

The bond angle and bond distances of the chlorobenzene and imidazole ring were used as the selected parameters in CTZ and were compared to other reported works. The bond length of the chlorobenzene ring (Table 2) showed a good agreement between the XRD [1] and the DFT. The C_{11}-C_1 which is the longest bond length was 1.743 and 1.764 for both XRD and DFT respectively. This was also in agreement to the single molecule of chlorobenzene which was determined experimentally to be 1.725 by Roussy et al [98] and theoretically calculated to be 1.762 [99], though at a lower basis set of 6-311G* as compared to the 6-311++G(d,p) basis set used in this work. The bond angle C_2-C_1-Cl_{11} was depicted to be 116° and 115.4° for the XRD and DFT respectively and this was lower compared to the single chlorobenzene molecule which was 119.801° and 119.308° for both the experimentally observed [98] and DFT calculated [99] respectively. The difference in bond angle is possibly due to the orientation of the chlorine atom to minimize the steric crowding due to the presence of the other three aromatic rings present in the title compound. For the imidazole ring, the DFT calculated bond lengths were slight higher than

the XRD. However, there was a very good agreement between N_{12}-C_{24} and N_{12}-C_{25} which were 1.372 and 1.315 respectively for the XRD and 1.375 and 1.314 for the DFT calculated. This also concurred to the experimental data [100] of single imidazole molecule and theoretically calculated [99] (though at a lower basis set of 6-311G**) which gave 1.314 and 1.312 respectively for N_{12}-C_{25}. The bond angles N_{10}-C_{23}-C_{24} and N_{10}-C_{25}-N_{12} had a perfect agreement in both the XRD and DFT of 106.1° for the former and a very good agreement of 112.5° and 112.3° for the latter respectively. This also concurred to the single imidazole theoretically calculated which gave 105.072° and 111.650° for N_{10}-C_{23}-C_{24} and N_{10}-C_{25}-N_{12} respectively.

Table 2. Some selected structural parameters of clotrimazole calculated using DFT/B3LYP at the 6311++G(d,p) basis set with XRD data.

Label	XRD	DFT
Bond length (Å)		
Cl_{11}-C_1	1.743 (2)	1.764
C_1-C_2	1.381 (3)	1.394
C_1-C_6	1.400 (3)	1.409
C_2-C_3	1.375 (3)	1.390
C_3-C_4	1.373 (4)	1.389
C_4- C_5	1.386 (3)	1.392
C_5-C_6	1.390 (3)	1.402
C_6-C_7	1.552 (3)	1.558
C_7-N_{10}	1.498 (2)	1.500
N_{10}-C_{23}	1.371 (3)	1.388
C_{23}-C_{24}	1.345 (3)	1.368
N_{12}-C_{24}	1.372 (3)	1.375
N_{12}-C_{25}	1.315 (3)	1.314
N_{10}-C_{25}	1.356 (3)	1.376
Bond Angle (°)		
C_2-C_1-Cl_{11}	116.0 (2)	115.4
C_6-C_1-Cl_{11}	122.1 (2)	122.7
C_2-C_1-C_6	121.9 (2)	121.9
C_3-C_2-C_1	120.0 (2)	120.3
C_3-C_4-C_5	120.0 (2)	120.0
C_4-C_5-C_6	121.8 (2)	122.5
C_6-C_7-N_{10}	106.7 (2)	109.6
N_{10}-C_{23}-C_{24}	106.1(2)	106.1
C_{24}-N_{12}-C_{25}	104.1 (2)	105.5
N_{10}-C_{25}-N_{12}	112.5 (2)	112.3

4.1.3 IR and Raman Spectra

The experimental Raman and IR bands (Figs 5 and 6) along with the calculated wavenumbers are depicted in Table 3. The wavenumbers were scaled using a factor of 0.961 for frequencies greater than 2700 cm^{-1} and 0.985 for frequencies less than 1800 cm^{-1} [93].. CTZ has 42 atoms and hence using the 3N-6 formula for the degree of freedom for a non-linear molecule, where N is the number of atoms it has 120 vibrational modes. The peak at 3302cm^{-1} are -CH stretch vibrations. This is because the vibration is symmetric and hence has a low activity in IR spectroscopy whereas it is highly active in Raman spectroscopy. The imidazole ring in CTZ has no N-H vibrations since the first Nitrogen atom is bonded to the quaternary carbon while the other is contributing to the aromaticity of the ring. The C-N stretch has been experimentally reported in imidazole to be in 1325 cm^{-1} to 1486 cm^{-1} [101] whereas it is observed to be in be at 1478 cm^{-1} and calculated to be at 1476 cm^{-1}. The difference in frequency is probably because of the quaternary carbon attached to the Nitrogen atom. The imidazole ring deformation was reported by Ramasamy to be at 891 cm^{-1} and 899 cm^{-1} for observed and calculated respectively [101]. However, in CTZ the imidazole ring deformation was seen at 883 cm^{-1} and 901 cm^{-1} for both observed and calculated respectively. The C-H stretch has been reported to be in the range of 3001-3091 cm^{-1} for Toluene [102]. Nevertheless, in CTZ the range is 3040- 3173cm^{-1} for the two benzene rings. However, at both 1156 cm^{-1} and 1145 cm^{-1} for both observed and calculated respectively, a C-H ring stretch is common to the three benzene derivatives simultaneously. The C-C ring stretch in Toluene is stated to be 1487-1624 cm^{-1} [102] while in CTZ it is observed to be in 1472- 1613 cm^{-1} for the two benzene rings. The chlorobenzene ring is responsible for the frequency observed at 1617 cm^{-1}. The ring deformation for the two benzene rings occurs at 1001 and 1002 cm^{-1} for both observed and calculated respectively this is much lower compared to what was reported for by Ramasamy

et al for Toluene [102] which occurs at 1032 and 1042 cm^{-1} for both observed and calculated respectively. The frequency seen at 1036 cm^{-1} is exclusively for the ring deformation of chlorobenzene. The Cl-C stretch was seen at 438, 434 and 447 cm^{-1} for the calculated, and experimentally determined IR and Raman respectively.

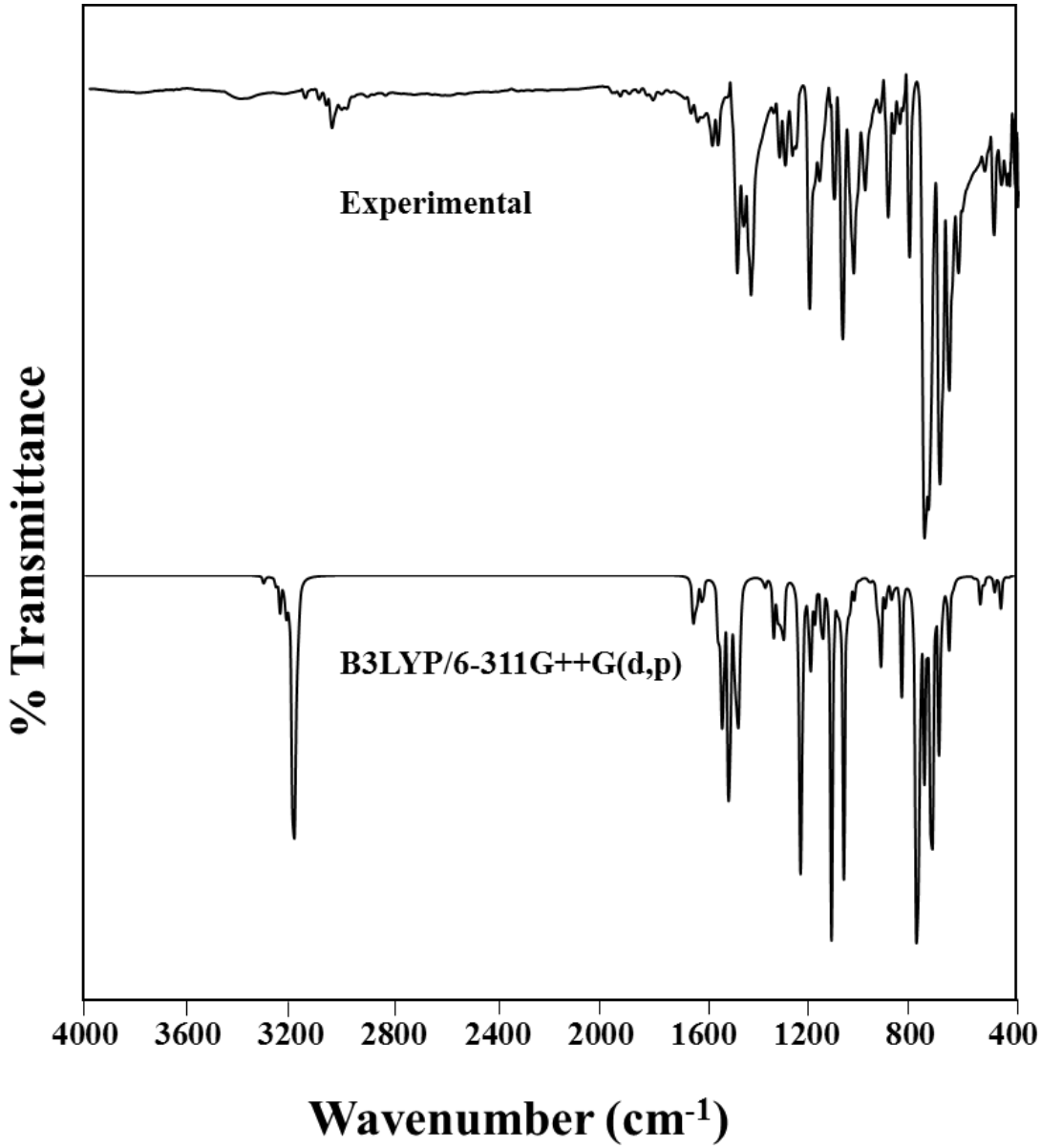

Figure 5. The IR spectra of CTZ

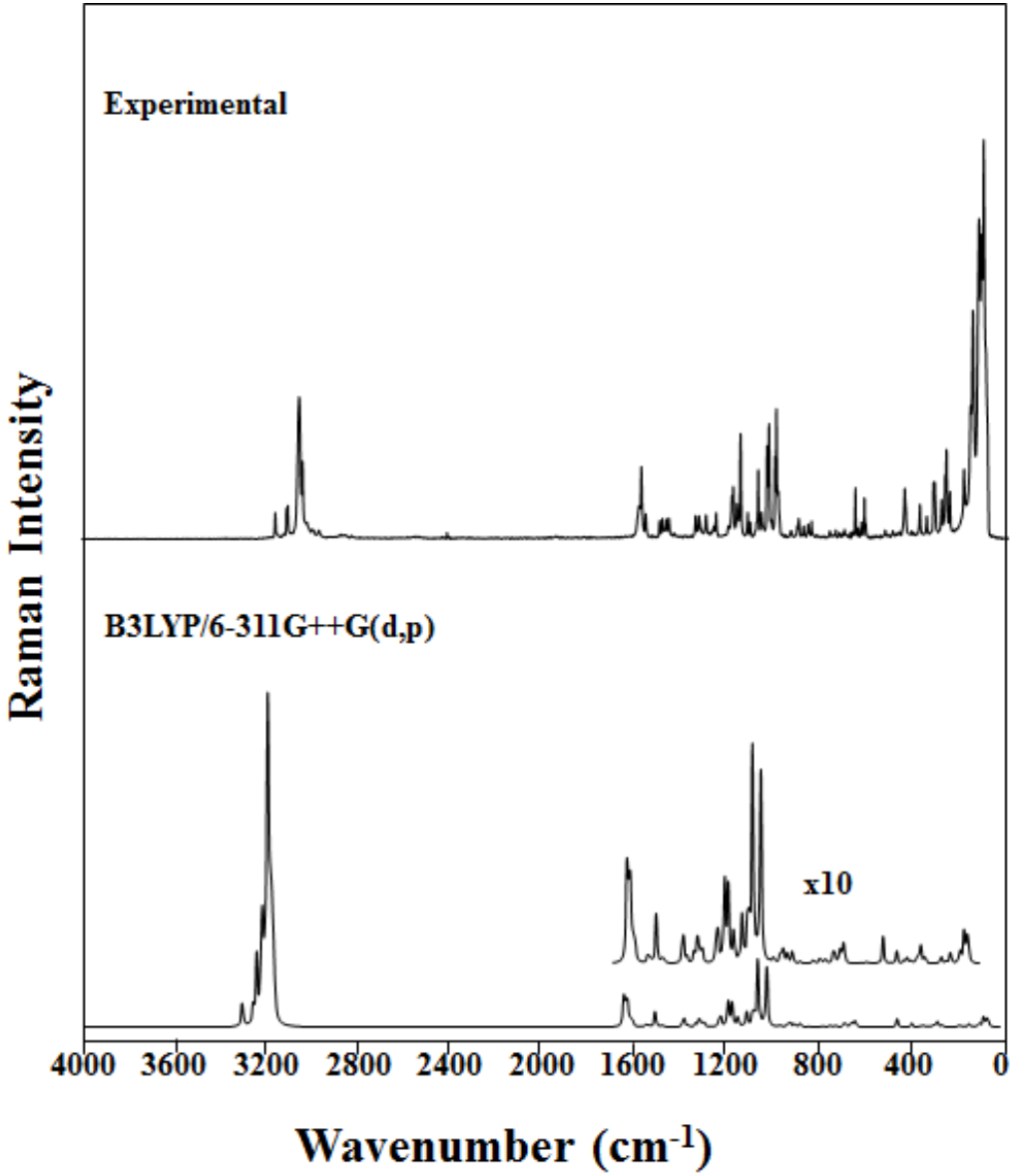

Figure 6. The FT-Raman spectra of CTZ

Table 3. Calculated and observed infrared, Raman frequencies (cm^{-1}), and vibrational assignments for clotrimazole

Calculated				Observed		
Sym.	Scaled Freq (cm^{-1}).	IR Int.	Raman Act.	IR (cm^{-1})	Raman (cm^{-1})	Assignment
A	3173.526	3.838	59.939	3164	3166	97% CH sym str
A	3134.548	0.611	33.010	-	-	99% CH sym str
A	3111.337	6.139	143.666	3110	3112	97% CH sym str
A	3093.172	0.829	136.966	-	-	82% CH sym str
A	3092.989	4.926	66.043	-	-	80% CH sym str
A	3089.065	3.137	89.999	3082	-	95% CH sym str
A	3077.598	4.010	174.616	-	-	78% CH sym str
A	3067.881	10.926	146.569	-	-	40% CH sym str
A	3066.992	10.412	332.581	-	-	31% CH sym str
A	3065.126	10.070	155.841	-	3063	53% CH sym str
A	3060.562	22.326	88.133	3061	-	37% CH sym str
A	3059.402	20.250	62.008	-	-	45% CH sym str
A	3051.101	2.266	66.999	-	-	53% CH sym str
A	3050.147	8.484	129.139	-	-	44% CH sym str
A	3048.924	5.964	116.974	-	3049	45% CH sym str
A	3041.044	0.119	41.838	-	-	38% CH sym str
A	3040.535	0.373	46.689	-	-	34% CH sym str
A	1617.597	1.953	20.880	1627	-	28% ring breadth
A	1613.609	4.862	33.103	-	-	21% sym ring str
A	1603.927	3.146	24.747	-	-	24% sym ring str
A	1599.329	1.206	20.310	-	-	20% sym ring str
A	1595.778	0.236	9.615	-	-	19% sym ring str
A	1580.799	5.457	14.520	1587	1585	33% sym ring str
A	1514.917	18.325	5.767	-		24% N-C str; 18% CH bend
A	1503.513	7.570	1.239	-	1506	14% ring breath
A	1502.462	22.410	0.357	1490	1494	13% ring breath

A	1476.056	20.700	18.533	-	1478	19% ring breath
A	1472.070	28.987	7.941	1466	-	17% ring breath
A	1456.836	15.638	1.090	-	-	13% ring breath
A	1449.998	8.552	1.135	-	-	14% ring breath
A	1439.663	33.602	0.399	1436	-	12% ring breath
A	1355.133	0.689	20.136	-	1351	47% N-C str
A	1344.594	0.538	1.117	1349	-	22% sym ring str
A	1338.681	0.551	1.690	1326	1336	23% sym ring str
A	1310.377	6.833	1.619	-	1306	12% asym ring str
A	1301.693	3.252	5.643	-	-	21% asym ring str
A	1295.868	10.539	8.168	-	-	11% N-C str
A	1283.454	5.075	4.414	-	-	13% asym ring str
A	1277.552	6.888	1.751	1276	-	33% asym ring str
A	1267.707	5.704	5.300	1271	1271	34% N-C asym bend
A	1201.256	18.181	6.379	1210	-	12% ring bend
A	1198.683	53.271	11.467	-	-	19% ring breath
A	1196.513	4.229	6.977	-	1193	18% CH asym bend
A	1181.188	6.142	12.480	-	1188	15% CC sym str; 24% CH asym. bend
A	1174.707	7.087	4.496	1171	1171	15% CC sym bend; 21% -CH asym bend
A	1167.151	0.552	2.284	-	-	29% CH asym bend
A	1166.798	0.042	3.082	-	-	33% CH asym bend
A	1164.270	4.799	3.474	-	1166	17% CC sym str; 13% CH asym bend
A	1145.774	8.530	43.027	-	1156	15% ring breath; 17% CH asym bend; 18% CC sym str
A	1134.455	7.451	3.361	-	-	18% ring breath; 25% CH asym bend
A	1122.622	13.037	3.391	1114	1114	45% N-C str; 31% CH asym bend
A	1099.413	1.882	0.481	-	-	11% ring breath
A	1094.768	1.513	0.899	-	-	10% ring breath
A	1079.087	68.887	18.154	1081	1080	13% ring breath; 48% CH asym bend

A	1060.069	3.551	27.990	-	-	32% ring breath; 20% CC sym str; 12% CH asym bend
A	1040.846	13.969	5.835	1039	-	15% ring breath
A	1038.514	1.952	65.053	-	-	16% ring breath; 20% CC asym str
A	1036.829	50.202	19.195	-	-	14% Cl-C sym str; 28% ring def
A	1016.050	4.811	6.504	-	-	34% N-C asym str;
A	1004.218	0.796	66.310	-	-	15% ring def
A	1002.458	2.248	6.000	-	1001	17% ring def,
A	997.079	0.046	5.471	-	-	40% CH twist
A	994.543	0.021	0.168	995	-	51% CH twist
A	986.865	0.114	0.032	-	-	76% CH twist
A	985.731	0.323	0.587	-	-	57% CH twist
A	980.242	0.536	0.471	-	-	60% CH twist
A	958.160	0.062	0.698	-	-	76 % CH twist
A	942.116	0.302	1.048	-	-	45 % CH twist
A	938.770	0.479	1.134	938	938	62% CH twist
A	917.797	7.344	3.801		-	11% CH twist; 15% ring breath; 33% CC sym str
A	903.646	11.971	4.494	905	904	20 % CC sym str; 11% ring breath; 11% CH wag
A	901.291	8.340	0.729	883	-	52% N-C ring breath
A	865.908	4.803	5.796		-	36 % N-C sym str; 10% CH twist
A	863.021	0.904	1.377		864	50 % CH twist
A	859.903	0.608	1.362	860	-	54% CH twist
A	853.208	0.467	0.049		-	49% CH twist
A	847.591	0.692	0.566	849	849	64% CH twist
A	821.967	20.975	0.770	823	-	74% CH wag
A	763.446	12.583	0.410	764	770	12% CH wag
A	755.799	55.417	0.509		-	57% CH wag
A	749.431	40.052	0.553		745	20 % CH wag
A	734.893	21.879	0.619		-	66% CH wag
A	728.307	3.890	0.549		-	28% CH twist

A	712.118	64.562	0.983		-	10% Cl-C sym str; 15% ring breath, 11% CH wag
A	710.053	31.196	0.469		707	11% CH wag
A	701.304	14.817	0.503	705	-	32% ring breath
A	676.056	11.828	6.303		681	26 % ring breath; 21% CH wag
A	666.747	13.922	3.952	669	660	13% ring breath; 29% CH wag
A	642.789	5.946	1.648		648	19% CH twist; 15% ring breath
A	638.744	9.153	3.490	633	634	26% ring breath; 10% CH wag
A	627.640	0.451	2.712	-	-	49% ring breath, 12% CH wag
A	623.786	0.527	3.632	-	-	64 % ring breath
A	620.859	0.893	4.129	620	621	25% N-C wag; 12% ring breath
A	540.857	0.893	0.255	531	531	22% CH twist; 11% CH wag
A	516.816	3.067	0.575	-	-	34% CH wag; 11% CH twist
A	505.983	1.096	0.558	495	498	17% Cl-C wag; 11% CH twist
A	465.239	3.399	0.137	466	-	19% CH twist; 31% Cl-C wag
A	438.359	5.473	6.772	434	447	41% Cl-C sym str; 17% ring breath
A	421.038	0.061	0.068	-	-	46% CH twist
A	411.586	0.489	0.209	412		47% CH twist
A	396.270	1.023	5.183	-		45% -Cl-C sym bend; 11% C-C bend
A	338.257	0.332	1.429	-		12% C-C asym bend; 33% N-C sym bend
A	317.007	0.690	2.018	-		10% C-C rock; 21% N-C wag
A	304.150	1.054	0.474	-		24% C-C asym str; 29% Cl-C bend scissors
A	294.938	0.448	3.045	-		11% out of plane ring def.; 13% Cl-C wag

A	289.721	0.091	2.579	-		11% C-C bend; 10% N-C bend
A	263.293	0.306	3.124	-		10% C-C bend; 10% N-C bend
A	258.312	0.375	1.194	-		19% C-C bend scissors; 10% -N-C bend
A	250.517	1.014	3.895	-		11% N-C bend scissors
A	176.884	0.222	2.180	-		24% C-C bend; 29% Cl-C wag
A	153.152	0.125	1.665	-		15% ring rock; 21% Cl-C twist
A	119.855	0.257	5.364	-		31% C-C out of plane bend; 14% N-C out of plane bend
A	107.287	1.094	1.018	-		10% N-C tors; 36% CC tors
A	95.706	0.669	0.622	-		25% C-C tors; 30% N-C tors
A	81.099	0.987	1.955	-		34% C-C tors; 18% N-C tors
A	73.731	0.453	8.034	-		36% CC tors; 15% NC tors
A	63.533	0.099	3.878	-		11% CCN rock; 10% CCC rock
A	58.757	0.231	3.460	-		27% N-C twist; 20% C-C twist
A	52.406	0.388	6.308	-		44% N-C twist; 10% C-C twist
A	37.707	0.526	0.355	-		25% C-C twist; 41% N-C twist

4.1.4 Frontier molecular orbitals

The HOMO (Highest Occupied Molecular Orbital) and LUMO (Lowest Unoccupied Molecular Orbital) are collectively known as the FMO (Frontier Molecular Orbital). They are an important quantum chemical parameter which help in understanding the bonding and adsorption properties of a compound especially when it comes to the use of compounds as corrosion inhibitors. The energy of the HOMO relates to ability of a compound to bind to a metal surface. A high HOMO energy indicates a good electron donation ability while a small HOMO-LUMO gap encourages the donation between the molecular orbitals of the compound and the orbitals of the metal surface such that a high adsorption will be detected [103]. The FMO values for CTZ are -6.155 eV and -1.277 eV for the HOMO and LUMO respectively while the energy band gap is 4.878 eV. It is observed that the HOMO occurs in the imidazole ring and this is mainly due to the presence of the nitrogen atoms while the LUMO occurs on the benzene rings which is due to the pi-electrons (Fig. 7). The FMO results indicated that CTZ has a good potential as a corrosion inhibitor and this has been reported in its ability to reduce the corrosion rate of Aluminum [63], [104].

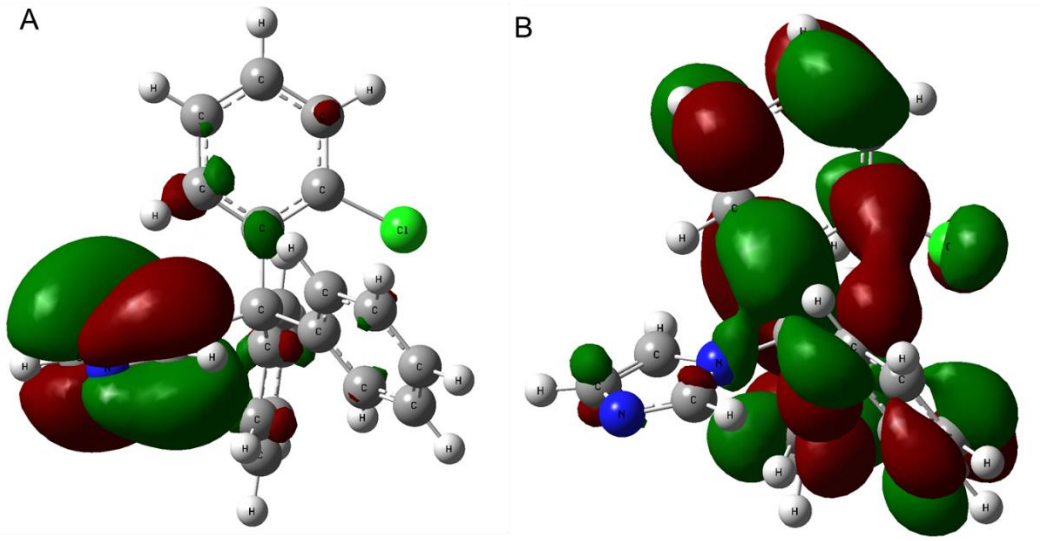

Figure 7. The HOMO (A) and LUMO (B) maps of CTZ

4.1.5 Molecular Electrostatic Potential

The Molecular electrostatic potential (MEP) map indicates the charge distribution in a molecule which is useful in knowing the potential sites for nucleophilic and electrophilic attacks. The blue region is positive and indicates nucleophilic reactivity while the red and yellow regions are negative and denote electrophilic reactivity. The electronegative regions occurred on N_{12} of the imidazole ring (red) and the chlorine atom (light yellow) though the former is more electronegative while the blue region occurred on the hydrogen atoms of the benzene rings (Fig. 8). The most reactive region of CTZ occurred on the nitrogen atom of the imidazole ring.

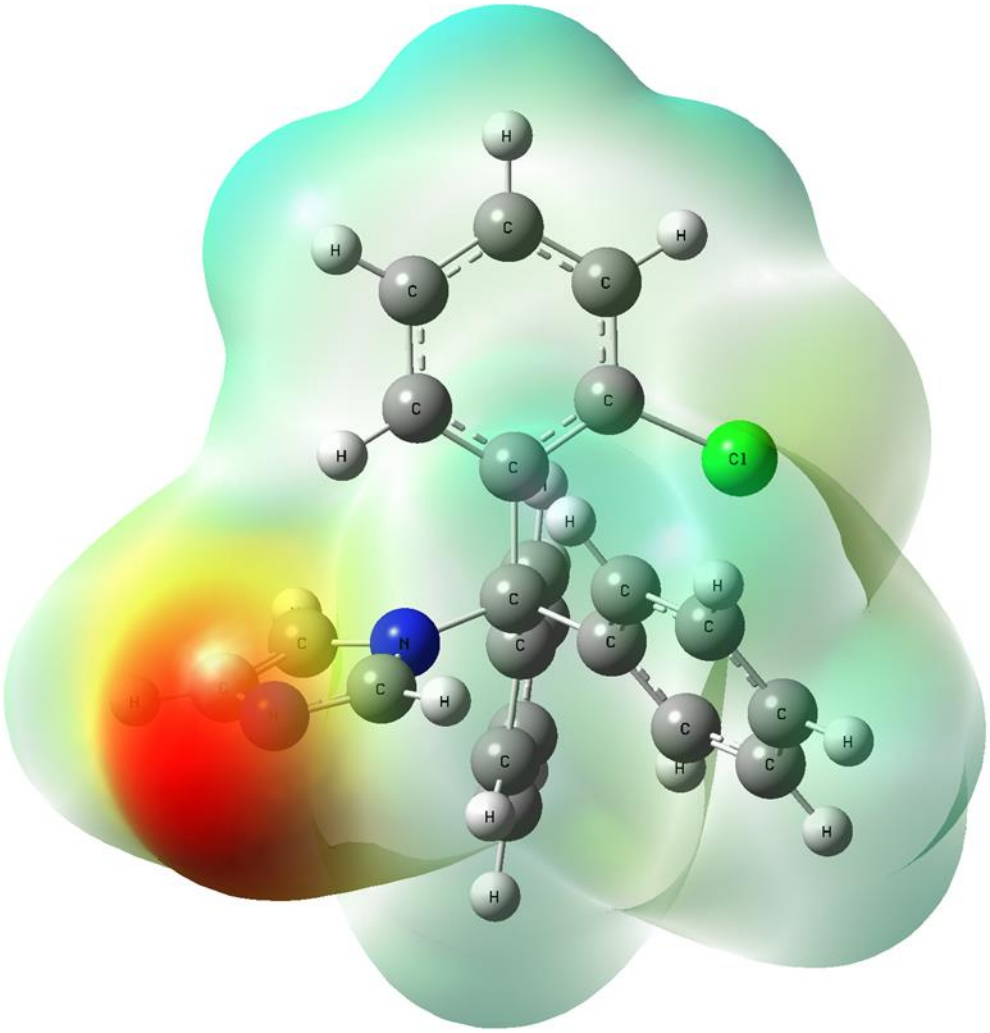

Figure 8. The MEP map of CTZ

4.1.6 Molecular docking studies

Recent studies [44], [45], [49], [105]–[107] suggest that secreted aspartic proteinases (SAPs), particularly SAPs 1-10 are virulent proteins which play an important role in the infection caused by *C. albicans* and hence should also be a drug target. These proteins are mostly found in the cell membrane [32] which implies they can easily interact with the host cells. Unfortunately, most of the crystal structure of the SAP proteins are not available in the protein database. For this study, the SAP2 protein was used with PDB ID: 1EAG [108]. Docking, which is the technique that predicts the best possible orientation known as a pose by which a ligand (drug) can interact a protein to form a steady complex [109]. This method is relatively new as it is one of the Computer Aided Drug Design (CADD) methods and it has also been used in the study of CTZ with CYP121 of another pathogen responsible for Tuberculosis, *Mycobacterium tuberculosis* [110]. MOLEMAN 2 was used to validate the target protein (SAP2) using Ramachandran plot (Fig. 9b). For a protein to be valid, it is recommended that the outlier percentage does not exceed 5% [111]. The outlier percentage of the target protein was detected to be 2.6% and hence was valid to be used for molecular docking analysis. The CLC drug discovery workbench program [96] was used for the molecular docking studies. The optimized structure of all the three conformers from Gaussian 09 were used as the ligand input file for the docking process while the complex A70450 present in the initial structure of the target protein was set as the reference ligand to establish the binding site (Fig. 9a) which gave the following binding parameters; 41.480, 22.670 and 12.460 for the X,Y and Z axes respectively. All the water molecules and ligand present in the initial structure were all removed from the target protein before docking the ligands and the docking was done with a radius of 13 Å in the binding site. The total docking score is a sum of the Hydrogen Bond (HB), Steric Interaction (SI) and ligand

Conformation Penalty (LCP) score values. All the three possible conformers showed good binding scores since they all had negative values when bound to the target protein. The steric interaction score had the highest contribution to the final docking score. Though, there was no significant difference in their score values (Table 4). The Drug discovery studio program [97] was used to visualize the binding mode and molecular interactions of CTZ with the target protein. However, since they all had similar docking scores only the binding mode of conformer B which is the most stable was depicted (Fig. 10). The molecular interactions of CTZ with the target protein includes two carbon-hydrogen bonds with SER 118 and ASP 120; Pi-alkyl interactions with ILE 30, ILE 119 and ILE 123; Pi-pi T-shaped interaction with TYR 84 and Pi-anion with ASP 120.

Table 4. The docking result of the clotrimazole conformations in SAP2 (PDB ID:1EAG) protein

Conformations	**HB Score**	**SI Score**	**Ligand conformation penalty**	**Final Docking Score**
A	0.00	-42.14	1.70	-40.44
B	-2.00	-39.86	1.63	-40.23
C	0.00	-41.47	1.70	-39.77

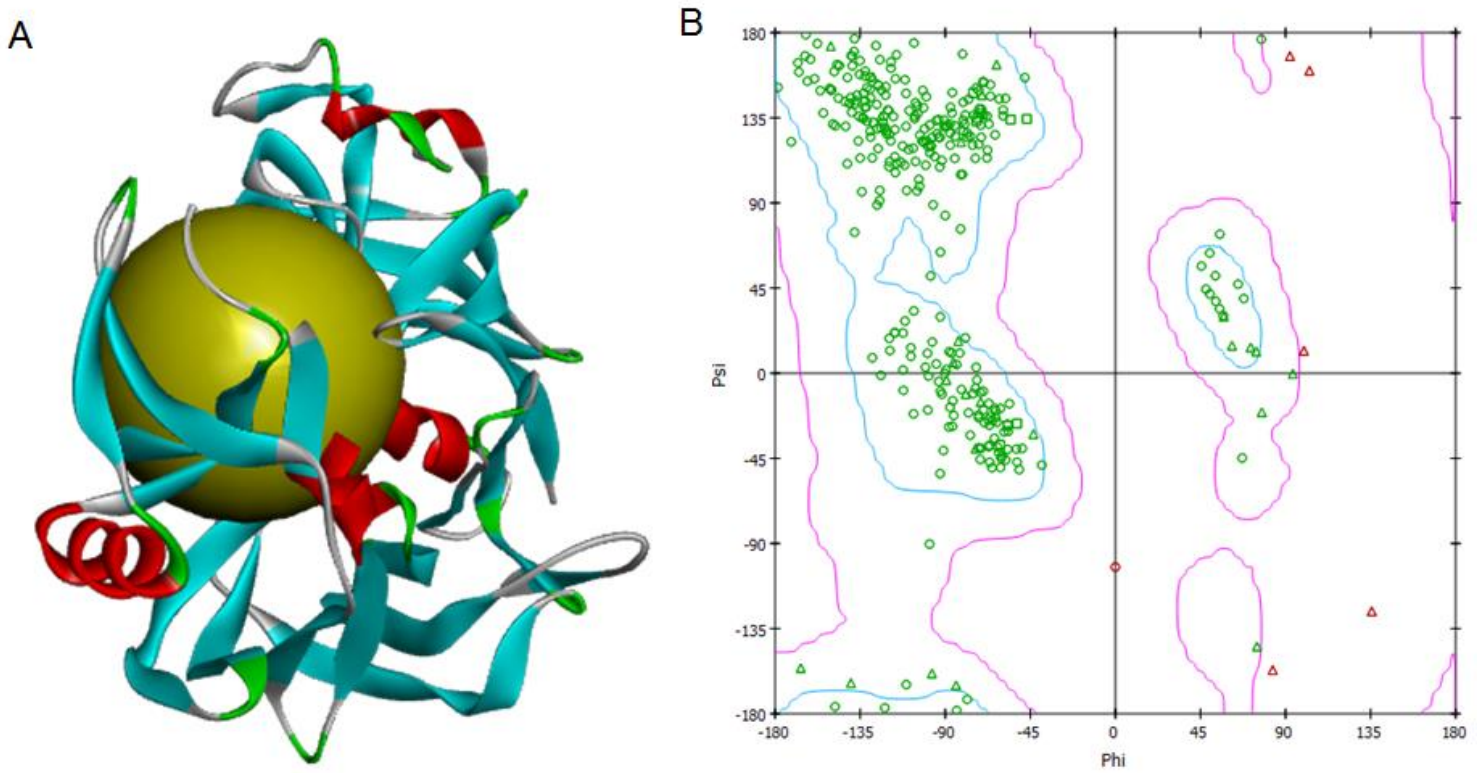

Figure 9. (A)The tertiary structure (binding site in yellow sphere) and (B) Ramachandran plot of the target protein SAP2 (PDB ID: 1EAG).

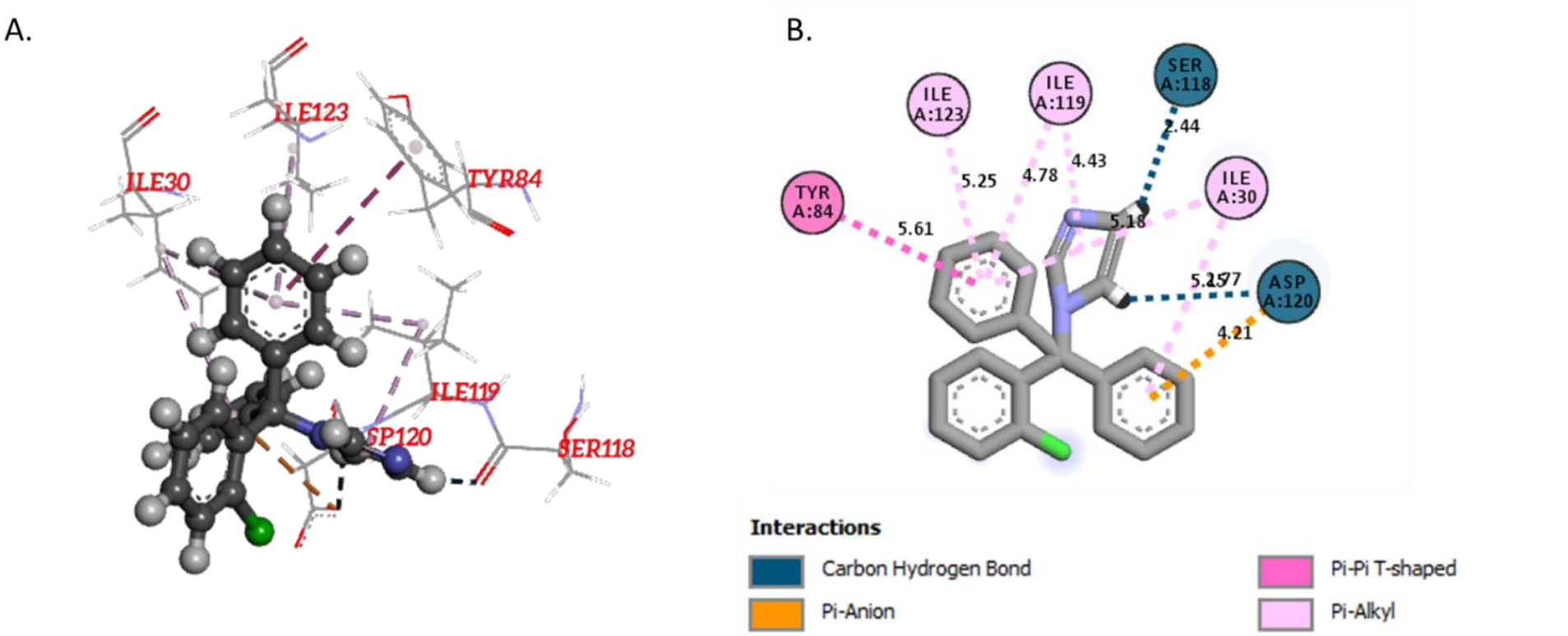

Figure 10. (A) The binding mode and (B) molecular interactions of the most stable conformer in SAP2 protein of *C. albicans* (PDB ID: 1EAG).

4.1.7 Conclusion

DFT studies using potential energy scan gave rise to three possible conformations of clotrimazole in both gas and aqueous phases. Extensive vibrational analysis was done to assign the spectroscopic bands. The molecular electrostatic map indicated that the positive region around the benzene rings while the negative region occurred on the imidazole ring. The frontier molecular orbitals revealed that the HOMO occurred on the imidazole ring while the LUMO occurred on the benzene rings. Molecular docking showed that all the possible conformers had good binding affinities with the target protein (SAP2). The molecular interactions include hydrogen bonding and steric interactions with the amino residues TYR, ASP and ILE present in the binding site. This molecular interactions could provide insight to the mode of action in which CTZ acts on *C.albicans* in treating candidiasis.

4.2 Resorcinol

4.2.1 Structure and vibrational properties

All theoretical levels employed in this study have predicted consistently that **AS** is the most stable form which is around 0.2 and 0.7 kcal/mol more stable than **A** and **S** forms, respectively. The prediction on the rotational constants with respect to the x, y and z coordinates are also in excellent agreement with experimental values (Table 6). Whereas the B3LYP level predicted the existence of three rotamers strictly planar with no imaginary frequencies, free-of-symmetry-constrain more accurate MP2 and MP4 optimizations predicted the hydroxyl group to very slightly tilt from the plane of the molecule. Like phenol, resorcinol in its electronic ground state adopts a planar configuration as it keeps the oxygen lone pairs of electrons in a position encountering the least possible intramolecular repulsion. The rotational barrier around the C-O bond predicted from the MP2 and B3LYP levels was found to be 3.5 and 3.8 kcal/mol, respectively.

To attain a better understanding of the nature of the intermolecular hydrogen bonding in the crystal phase of resorcinol and the bioactivity of the resorcinol molecule towards the target protein, we focused on the conformational properties arising particularly from the internal rotation by the two hydroxyl groups. The derived PES scan (Fig. 14) in terms of both CC-OH dihedral angles (denoted as φ_1 and φ_2) revealed that in non-condensed phases resorcinol molecule interchanges from one form into another through the **AS** route, i.e., in the **AS** ↔ **A** ↔ **AS** or **AS** ↔ **S** ↔ **AS** interchange patterns. On the other hand, at least 7 kcal/mol is required for the **A** ↔ **S** ↔ **A** or **S** ↔ **A** ↔ **S** types of conformational interchange which is less likely to take place. The MP2/6-311++G(d,p) characterized the

three possible minimum forms to be more flat than that predicted by the B3LYP/6-311++G(d,p) level of theory. This supported the assumption that the molecule in the solid lattice is capable of adopting an internal arrangement that maximizes the extent of the intermolecular hydrogen bonding, whose influence in turn can be clearly observed from its high melting point and low solubility. The structural parameters of the optimized unit cell of α-resorcinol were in good agreement with those have been determined by the x-ray experiment [112] Furthermore, the unit cell (Fig. 11) adopts an overall near C_s symmetry, wherein some of the hydroxyl groups tend to deviate from planarity (Table 7) to facilitate O-H···O intermolecular bonding. The difference between the calculated non-bonded H···O distances (in the order of 1.9 Å) and that reported experimentally (1.7 Å [112]) implies the very strong packing forces facilitated by intermolecular hydrogen bonding in resorcinol.

The comparison between the calculated B3LYP/6-311++G(d,p) and the experimental (gas [10] and solid [32]) bond lengths, bond angles and dihedral angles of the most stables forms of resorcinol (anti **A** and anti-syn **AS**), its dianion salt and the α-unit cell has been listed in Table 7. The bond lengths and most of the bond angles do not vary much between the two rotameric forms, nor deviate much from those reported for the solid phase. The changes of the structural properties for the benzene ring in going from resorcinol to its dianion salt are quite interesting and some insights could be noticed by carefully comparing the obtained computational and spectroscopic data. The aromatic C-C bonds in the dianion salt were predicted to be in average 0.05 Å longer than compared to the parent molecule. The transformation to the dianion form makes the electron pairs on oxygen tend to delocalize more, resulting in the development of a trace π-character across the C-O bonds, which in turn distort the uniformity of the electron density of the benzene

ring. This can be viewed from the variation in the calculated C-C bond distances and CCC angles as well as from the lesser sp^2 character depicted by the deviation of the hydrogen atoms from the planar configuration. The observed shifts in the infrared and Raman spectral bands associated with the ring and C-O modes (Tables 8-10) support the calculation findings and are clarified further in the next section. The ^{1}H NMR data support the structural influence of abstracting the hydroxyl hydrogens from the resorcinol ring. The resonance peak at δ 4.72 ppm due to hydrogen of hydroxyl function in resorcinol disappeared in both resorcinol-OD and dianion. In addition, the aromatic signals in dianion exhibited slight upfield shift compared to parent compound. This was indicative of electron shielding effect due to increased flux of electron density from oxygen lone pairs into the aromatic ring.

The assignments of local vibrational modes of resorcinol, its deuterated isotopomer and dianion salt derivatives in the solid phase were given in Tables 3-5. While a number of reports had proposed the vibrational assignments of resorcinol in the condensed and gas phases [6, 11,13,15,24,25,26,29] , the assignments presented here were made on a comparative basis with resorcinol derivatives. An overview of the previous infrared and Raman vibrational assignment reports [76] performed on resorcinol showed that most of the features of the solid-phase and gas-phase spectra are of high similarities. In the current study, the assignments of vibrational modes associated with the hydroxyl groups were affirmed by monitoring the isotopic shifts in the spectra the -OD isotopomer and the disappearance of such modes in the dianion salt spectra, supported by theoretical frequencies. To insure more reliable assignments and account for possible intermolecular interactions, the infrared and Raman wavenumbers of α-resorcinol and its –OD derivative

were compared with the calculated ones for the optimized unit cell structure (Tables 8 and 9).

The 36 vibrational modes in resorcinol and its -OD derivative, which adopt C_{2v} symmetry for the **A** form, span the irreducible representations: 13 A_1 + 4 A_2 + 12 B_1 + 7 B_2, while in the case of the dianion salt, due the absence of the two alcoholic hydrogens, there are 30 vibrational modes that span the irreducible representations: 11 A_1 + 3 A_2 + 10 B_1 + 6 B_2. According to the symmetry selection rules A_2 modes are expected to be only Raman active. However, since in the solid phase resorcinol was reported [33] and calculated at the MP2 and MP4 levels to be slightly non-planar, some of the A_2-symmetry modes, namely ν_{14} and ν_{15}, absorb very weekly in the infrared spectra. Such modes, however, could be located for the dianion salt only in the Raman spectrum due to its strictly planar configuration. Calculated frequencies for single molecules agree in most of the cases with those experimentally observed in the solid phase vibrational spectra. However, the values of some of the computed frequencies were noticed to be smaller than the corresponding observed ones. These vibrations belong mainly to A_2 and B_1 symmetries which describe out-of-plane modes. The higher experimental values of the solid phase facilitated by strong packing forces are somehow due to hindrance of out-of-plane vibrations and hence requires slightly greater vibrational energies. This motivated us to recalculate the vibrational frequencies for α-resorcinol (rotamer **A**) but in the environment of the unit cell (Fig. 11) rather than a single molecule. The deviated frequencies in the case of the isolated molecular system were improved and showed better agreement with experimental values of the solid phase especially for the bending modes below 1000 cm^{-1} (Tables 8 and 9). For instance, the O-H wagging (O-D wagging for the OD isotopomer) mode, ν_{16} , were calculated to be

in the range of 337-350 cm^{-1} (250-252 cm^{-1}) in the case of unit cell and 304 cm^{-1} (219 cm^{-1}) for isolated molecules, compared to the observed 358 cm^{-1} (249 cm^{-1}) values.

The observed broad infrared band nearly at 3180 cm^{-1} which is associated with the stretching modes of the intermolecular hydrogen-bonded –OH group was shifted upon deuteration down to 2387 cm^{-1} with the band pattern and intensity being retained indicating the existence of appreciable hydrogen bonding in the case of the isotopomer sample. The asymmetric and symmetric O-D stretching vibrations were resolved in the Raman spectrum as by the weak lines observed at 2452 cm^{-1} and 3033 cm^{-1}, respectively. The in-phase in-plane O-H wagging mode observed as a medium intensity infrared band at 1166 cm-1 (DFT is 1188 cm^{-1}) in the resorcinol spectrum was shifted to 951 cm^{-1} (DFT is 929 cm^{-1}) as a strong infrared band in the spectrum of the isotopomer derivative. The isotopic shifts associated with the hydroxyl groups in the solid phase and defined as $\nu_{Resorcinol}/\ \nu_{Resorcinol\text{-}OD}$ were found to be greater for the stretching vibrations (1.33) compared to the bending ones (1.23) which could be attributed to the more significant involvement of the stretching modes in the hydrogen bonding compared to the corresponding bending ones.

Moreover, some vibrational frequency shifts were noticed because of the abstraction of the acidic protons from the resorcinol molecule (Figs. 12 and 13). The C-O in-phase (ν_7 at 1281 cm^{-1} with 67% PED) and out-of-phase (ν_{27} at 960 cm^{-1} with 33% PED) were shifted to higher frequencies (1404 and 1236 cm^{-1}, respectively) and become less coupled with other modes (75% calculated PED vales). This is due, as indicated earlier, to the more pronounced π-electron character associated with the C-O bonds and hence shorter bond lengths in the case of the dianion salt. This is accompanied with non-uniformity of the electron cloud across the benzene ring as supported by noticeable downward shifts of

the observed wavenumbers for the C-C stretching as going from resorcinol to its dianion derivative. For instance, the ring breathing mode observed as the strongest Raman line at 998 cm^{-1} for resorcinol has shifted to 977 cm^{-1} in the Raman spectrum of the dianion salt (Fig. 13). This is also true for other ring stretching modes such as ν_5 , ν_6 , ν_{20} and ν_{21} . Optimized DFT structures (Table 7) predicted an average increase in the C-C bond distance from 1.40 to 1.45 Å, and a decrease in the C-O bond distance from 1.356 to 1.296 Å, in going from resorcinol to its dianion salt. In addition, the C-H bonds was shown to be slightly less stiff in the case of the dianion salt where they absorbed as low as 2978 cm^{-1} in the infrared spectrum with excellent agreement with the theoretical values (Table 10).

Table 5. Calculated relative stabilities (kcal/mol) for the anti-syn (AS), anti (A) and syn (S) conformations of resorcinol[1].

	B3LYP		**MP2**		**MP4SDQ**	
Rotamer	**6-311G**	**6-311++G**	**6-311G**	**6-311++G^2**	**6-311G**	**6-311++G**
AS	0.000	0.000	0.000	0.000 (*0.000*)	0.000	0.000
A	0.188	0.112	0.210	0.103 (*0.109*)	0.230	0.132
S	0.689	0.730	0.704	0.733 (*0.745*)	0.715	0.746

1.The calculated structures at the MP2 and MP4 levels are for *C*1 symmetry of resorcinol.

2.Values in brackets are calculated for strictly planar structures of resorcinol

Table 6. Rotational Constants calculated at different levels of theory for the anti-syn (AS), anti (A) and syn (S) conformations of resorcinol in GHz compared with experimental values.

		Coordinates					
		6-311G(d,p)			6-311++G(d,p)		
	Rotamer	X	Y	Z	X	Y	Z
Experimental	AS	3.758	1.831	1.231	-	-	-
	A	3.755	1.834	1.233	-	-	-
	S	3.766	1.824	1.229	-	-	-
B3LYP	AS	3.766	1.830	1.232	3.737	1.802	1.225
	A	3.762	1.834	1.233	3.758	1.833	1.232
	S	3.776	1.823	1.230	3.772	1.822	1.229
MP2	AS	3.748	1.824	1.227	3.742	1.822	1.225
	A	3.738	1.829	1.228	3.719	1.812	1.223
	S	3.766	1.815	1.225	3.759	1.812	1.223
MP4SDQ	AS	3.751	1.826	1.228	3.745	1.824	1.227
	A	3.746	1.829	1.229	3.740	1.829	1.228
	S	3.760	1.819	1.226	3.755	1.817	1.225

Table 7. Structural parameters of the Resorcinols A, AS and the α-unit cell from both observed and calculated at the B3LYP/6-311++G (d,p) levels of theory. All bond lengths are in Å and angles in degrees

	A		AS		α-Unit Cell		
Bond Lengths	**Obs. [a]**	**Calc.**	**Obs. [a]**	**Calc.**	**Obs.[b]**	**Calc.[c]**	**Salt**
C_1 - C_2	1.394	1.396	1.388	1.4	1.396	1.393	1.436
C_2 - C_3	1.396	1.401	1.388	1.397	1.399	1.398	1.451
C_3 - C_4	1.407	1.397	1.408	1.402	1.397	1.392	1.402
C_4 - C_5	1.407 [b]	1.397	-	1.393	1.393	1.392	1.402
C_5 - C_6	1.396 [b]	1.401	-	1.402	1.400	1.398	1.451
C_6 - C_1	1.394 [b]	1.396	-	1.395	1.395	1.393	1.436
C_1 - H_{11}	1.086	1.085	1.091	1.087	1.088	1.083	1.094
C_2 - O_7	1.357	1.369	1.371	1.37	1.378	1.371	1.296
C_3 - H_9	1.086	1.087	1.091	1.087	1.089	1.084	1.092
C_4 - H_{12}	1.086	1.087	1.091	1.087	1.087	1.084	1.099
C_5 - H_{10}	1.086	1.087	1.091	1.085	1.087	1.085	1.093
C_6 - O_8	1.357	1.369	1.371	1.369	1.374	1.371	1.296
O_7 - H_{13}	0.955	0.96	0.959	0.96	1.003	0.966	-
O_8 - H_{14}	0.955	0.96	0.959	0.96	1.005	0.966	-
Bond Angles							
C_1-C_2-C_3	120.68	120.92	120.68	120.8	121	120.32	115.2

C_2-C_3-C_4	119.41	118.93	119.41	118.9	118.5	119.51	120.2
C_3-C_4-C_5	120.14	121.12	120.14	121.4	121.6	121.12	123
C_4-C_5-C_6	119.41[c]	118.91	-	118.8	118.8	119.03	120.2
C_5-C_6-C_1	120.68[c]	120.92	-	120.9	120.7	120.32	115.2
C_6-C_1-C_2	119.68	119.21	-	119.3	119.3	119.12	125.7
C_3-C_2-O_7	119.6	122.33	119.6	122.8	122.4	121.83	121.5
C_5-C_6-O_8	122.18	122.33	119.6	117.1	122	121.83	121.5
C_2-C_1-H_{11}	120.16	120.42	120.16	119.2	120.2	120.42	117
C_6-C_1-H_{11}	120.29	120.42	-	121.5	120.5	120.42	117
C_2-O_7-H_{13}	108.55	108.63	-	108.5	111.8	109.92	-
C_6-O_8-H_{14}	108.55 [c]	108.63	-	108.8	111.8	109.91	-
C_2-C_3-H_9	120.29	120.42	-	120.4	120.9	120.42	118.2
C_6-C_5-H_{10}	120.29 [c]	120.42	-	119.4	120.8	120.42	118.2
Dihedral Angles							
C_3-C_2-O_7-H_{13}	-	0	-	180	6.9	4.75	-
C_5-C_6-O_8-H_{14}	-	0	-	0	9.7	5.21	-
C_5-C_6-C_1-H_{11}	-	-180	-	180	180	180	180
C_2-C_3-C_4-H_{12}	-	180	-	180	180	180	180
C_1-C_2-C_3-H_9	-	180	-	180	180	180	180
C_1-C_6-C_5-H_{10}	-	180	-	180	180	180	180

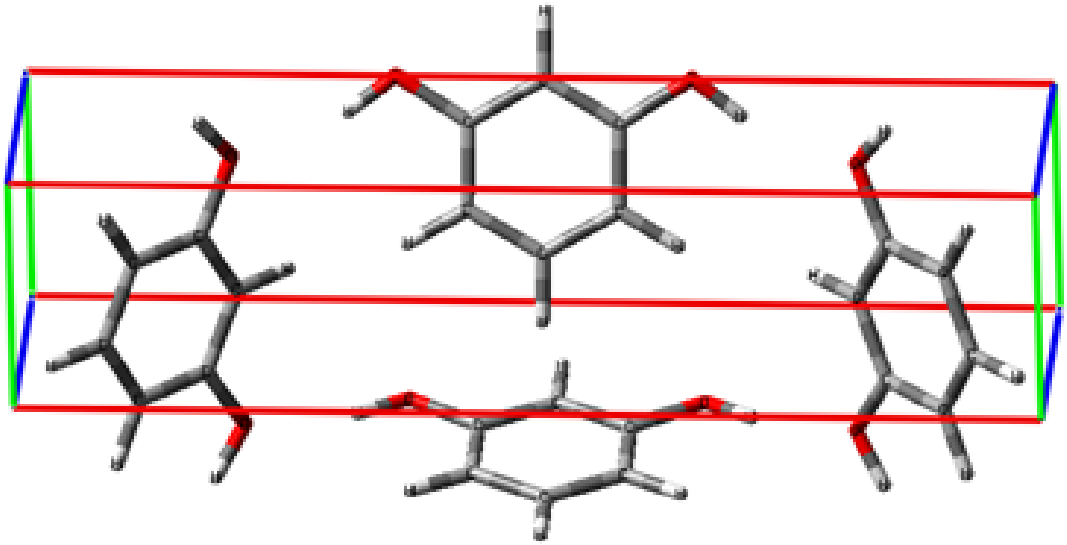

Figure 11. Structure of α-resorcinol unit cell as optimized at the B3LYP/6-311g(d,p) level of theory

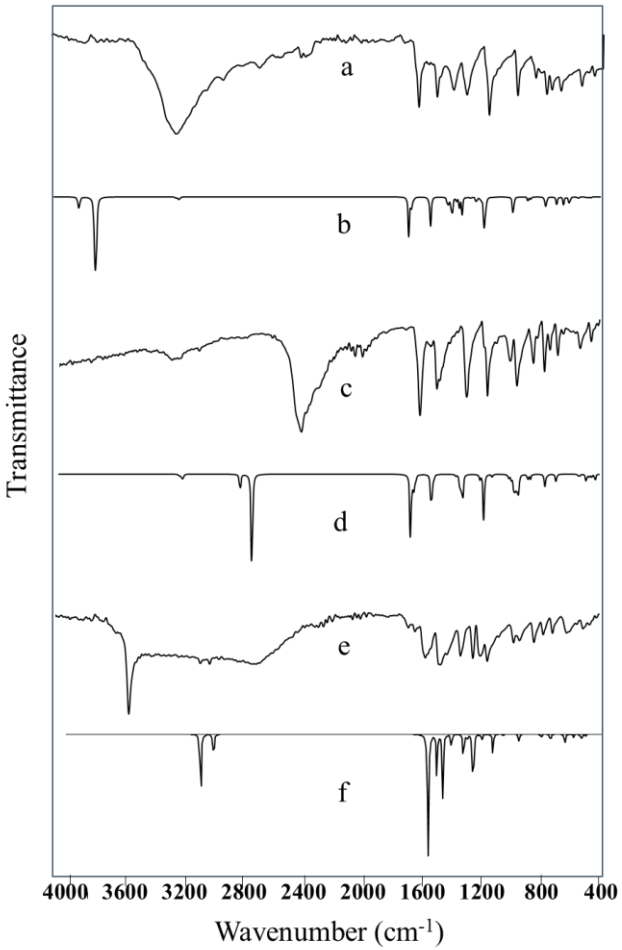

Figure 12. Mid-infrared spectra of (a) α-resorcinol (solid), (b) α-resorcinol unit-cell (calculated), (c) α-resorcinol-OD isotopomer (solid), (d) α-resorcinol-OD isotopomer unit-cell (calculated), (e) resorcinol dianion salt (solid), and (f) resorcinol dianion salt (calculated).

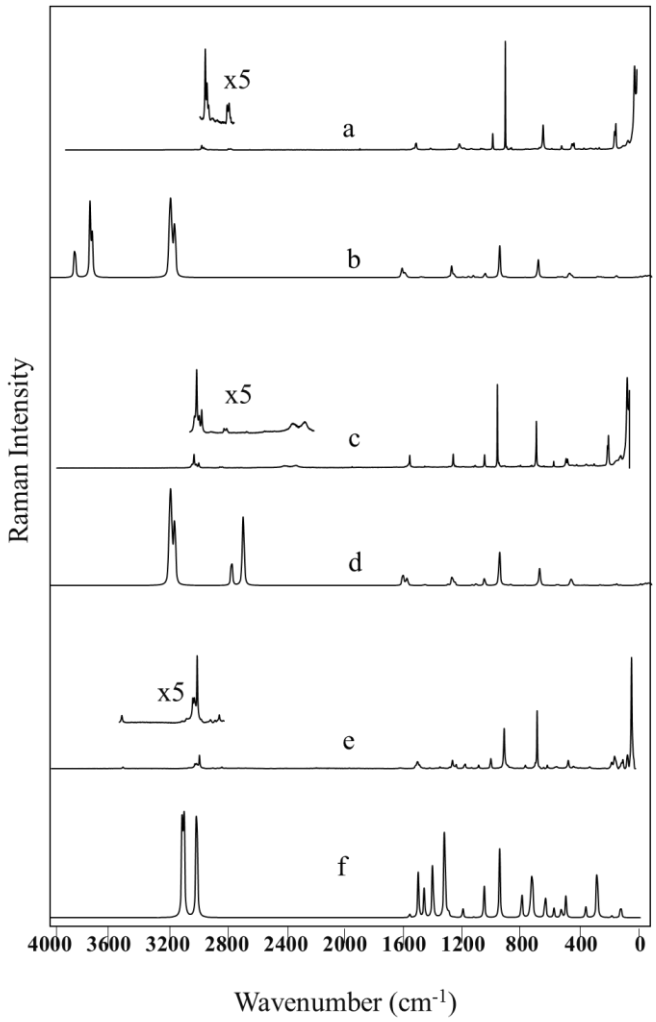

Figure 13. Raman spectra of (a) α-resorcinol (solid), (b) α-resorcinol unit-cell (calculated), (c) α-resorcinol-OD isotopomer (solid), (d) α-resorcinol-OD isotopomer unit-cell (calculated), (e) resorcinol dianion salt (solid), and (f) resorcinol dianion salt (calculated).

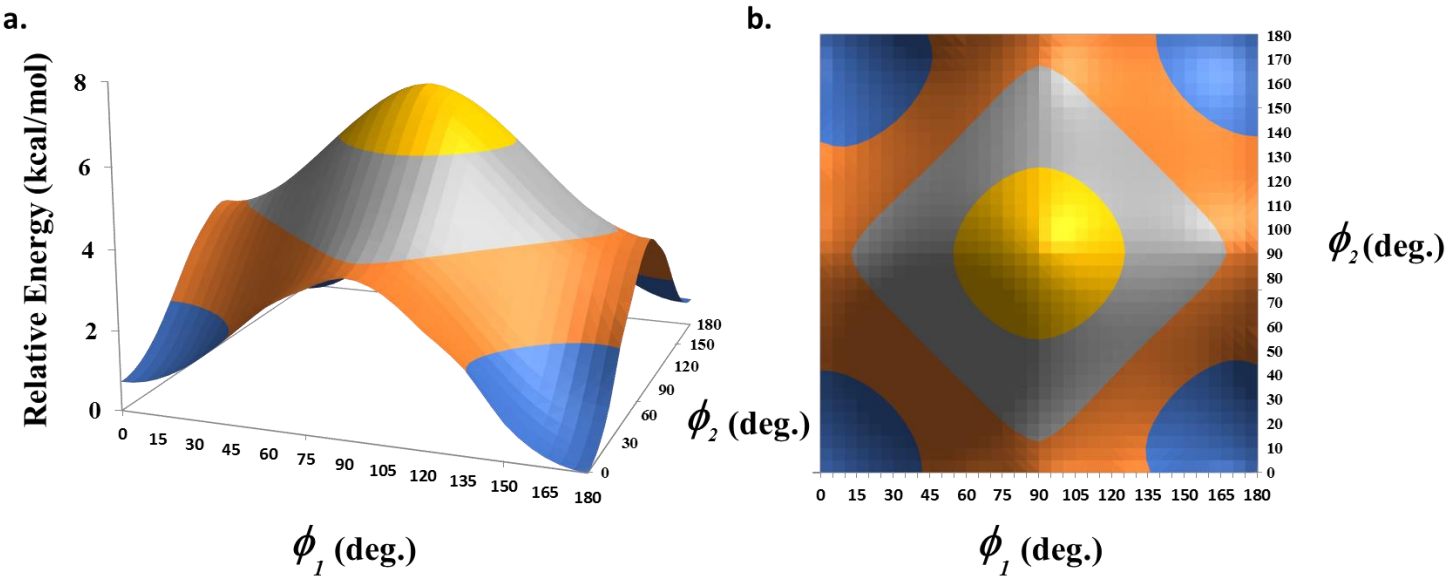

Figure 14. (a) 3D potential energy scan and (b) contour plot describing the relative energy changes with respect to the internal rotation of the hydroxyl groups (ϕ_1 and ϕ_2) in resorcinol**.**

Table 8. Experimental and calculated wavenumbers of resorcinol.

Sym	Description	Calculated		Experimental		
		DFT/B3LYP				
		Single molecule (cm^{-1})	**Unit cell** (cm^{-1})	**DF for single molecule (gas)**[c] (cm^{-1})	**IR (solid)** (cm^{-1})	**Raman (solid)** (cm^{-1})
A_1	ν_1 O-H str.(100%)	3704	3582-3699		~3183 vs,br	
	ν_2 C-H str.(100%)	3095	3090-3093			3071 ms
	ν_3 C-H str.(93%)	3074	3073-3082			3056 ms
	ν_4 C-H str. ip (93%)	3047	3044-3056			3043 w
	ν_5 Ring str.(65%)	1614	1605-1622	1617	1605 s	1604 m
	ν_6 Ring str.(40%)	1507	1505-1515	1509	1508 vw	1509 w
	ν_7 C-O str. ip (67%)	1303	1291-1308	1305	1281 ms	1280 w
	ν_8 O-H wag ip (74%)	1188	1198-1202	1196	1166 m	1167 w
	ν_9 C-H wag ip (41%)	1090	1088-1092	1083	1083 w	1084 ms
	ν_{10} Ring breath(45%)	994	993-997	999	998 vw	998 vvs

	ν_{11} Ring bend(27%)	742	740-745	740	739 m	740 s
	ν_{12} Ring bend(62%)	538	536-541	534	543 m	544 m
	ν_{13} CCO def. ip (77%)	328	333-361	329	421 w	~417 w,br
A_2	ν_{14} C-H wag op(76%)	805	527-833		801 vvw	~798 vvw,br
	ν_{15} Ring def.(76%)	610	603-634		612 w	614 m
	ν_{16} O-H wag op (95%)	304	337-350,584,663			358 w
	ν_{17} Ring def. (76%)	227	231-237			244 s
B_1	ν_{18} O-H str. op (100%)	3704	3582-3699		~3183	
	ν_{19} C-H str. op (100%)	3052	3056-3065			3116 w
	ν_{20} Ring str. (66%)	1637	1632-1635	1636	1622 m	1624 m
	ν_{21} Ring str. (100%)	1495	1491-1500	1492	1484 s	
	ν_{22} Ring str.(56%)	1350	1351-1384	1353	1374 ms	~1373 vvw,br
	ν_{23} C-H wag op (64%)	1324	1326-1328	1320	1310 m	1312 m
	ν_{24} O-H wag op (31%)	1207	1231-1260	1207		~1230 w,br
	ν_{25} C-H wag(68%)	1165	1165-1170	1179		1162 w

	ν_{26} C-H wag(36%)	1137	1137-1151	1134	1147 s	1143 vw
	ν_{27} C-O str. $_{op}$(33%)	958	954-963	936	960 ms	957 w
	ν_{28} Ring bend (74%)	522	521-527	520		530 m
	ν_{29} CCO def. $_{op}$(84%)	468	471-487	475		499 vw
B_2	ν_{30} C-H wag (86%)	912	943-952	905	~92 vw,b	
	ν_{31} C-H wag (68%)	835	845-864	846	841 m	~844 vw,br
	ν_{32} C-H wag $_{ip}$ (83%)	723	747-753	729	771 ms	766 w
	ν_{33} Ring def. (59%)	629	676-682	611	681 m	678 w
	ν_{34} Ring def. (80%)	449	456-459	437	461 m	459 w
	ν_{35} O-H wag $_{ip}$ (97%)	293	321-323,594,637			
	ν_{36} Ring def. (95%)	216	226-231			193 w

* Given in terms of a C_{2v}-symmetry structure.
** Abbreviations: ip = in-phase, op = out-of-phase,
[b] The calculated wavenumbers are scaled and are for rotamer **A** with C_{2v} symmetry.
[c][12]

Table 9. Experimental and calculated wavenumbers of resorcinol-OD.[a]

Sym	Description	Calculated		Experiment(Solid)	
		B3LYP			
		Single (cm^{-1})	**Unit Cell** (cm^{-1})	**IR** (cm^{-1})	**Raman** (cm^{-1})
A_1	ν_1 O-D str.(100%)	2696	2609-2693	2387 vvs	2452 w,br
	ν_2 C_1-H str.(100%)	3095	3090-3093	3068 m	3066 ms
	ν_3 C_4-H str.(93%)	3074	3073-3082		3050 w
	ν_4 C-H str. $_{ip}$ (93%)	3047	3049-3056		3034 m
	ν_5 Ring str.(65%)	1604	1595-1612	1597 vs	1597 ms
	ν_6 Ring str.(65%)	1481	1480-1481	1465 s	1468 vw
	ν_7 C-O str. $_{ip}$ (40%)	1303	1299-1307		1301 ms
	ν_8 O-D wag $_{ip}$ (83%)	914	921-929	951 s	~953 vw,br
	ν_9 C-H wag $_{ip}$ (44%)	1095	1091-1097	1086 w,br	1087 ms
	ν_{10} Ring breath (45%)	995	994-998		999 vvs

	ν_{11} Ring bend (43%)	733	731-737	730 m	734 vs
	ν_{12} Ring bend (62%)	527	526-532	529 m	532 m
	ν_{13} CCO def. ip (77%)	312	316-335		395 w
A_2	ν_{14} C-H wag op (76%)	806	827-833	793 vvw	
	ν_{15} Ring def. (76%)	608	611-622		616 m
	ν_{16} O-D wag op (95%)	219	250-252,422,442		341 w
	ν_{17} Ring def. (76%)	232	206-228		180 w
B_1	ν_{18} O-D str. op (100%)	2696	2609-2693	2387	2452
	ν_{19} C-H str. op (100%)	3052	3056-3065		3080 w
	ν_{20} Ring str. (66%)	1632	1625-1634		1612 sh
	ν_{21} Ring str. (100%)	1494	1491-1499	1484 s	
	ν_{22} Ring str.(56%)	1334	1332-1334	1339 vw	1330 vw
	ν_{23} C-H wag ip (64%)	1296	1288-1297	1286 s	1285 vw
	ν_{24} O-D wag op (36%)	920	942-967		
	ν_{25} C_4-H wag (31%)	1173	1173-1177	1169 sh	1167 vw
	ν_{26} C_1-H wag (68%)	1150	1146-1152	1147 s	1150 w

	ν_{27} C-O str. $_{op}$ (33%)	971	967-988	995 ms	989 m
	ν_{28} Ring bend (74%)	517	515-521		521 m
	ν_{29} CCO def. $_{op}$ (84%)	443	461-483		490 vw
B_2	ν_{30} C_4-H wag (86%)	912	943-952		
	ν_{31} C_1-H wag (68%)	834	844-862	841ms	842 w
	ν_{32} C-H wag $_{ip}$ (83%)	723	746-752	767 ms	766 w
	ν_{33} Ring def. (59%)	629	676-680	678 ms	681 w
	ν_{34} Ring def. (80%)	449	457-459	455 m	460 w
	ν_{35} O-D wag $_{ip}$ (95%)	189	263-266,420,445		
	ν_{36} Ring def. (97%)	240	222-232	2495	

[a] See footnotes of Table 8.

Table 10. Experimental and calculated wavenumbers of the resorcinol dianion salt.

Sym.	Description	Calculated DFT/B3LYP (cm^{-1})	Experiment (solid)	
			IR (cm^{-1})	Raman (cm^{-1})
A_1	ν_1 O-H str.	-		
	ν_2 C-H str.(90%)	2980		3012 m
	ν_3 C-H str.(93%)	2902	3041 vm	3042 w
	ν_4 C-H str. $_{ip}$ (84%)	2992	2978 vm	
	ν_5 Ring str.(31%)	1482	~1461 ms,br	1475 vm
	ν_6 Ring str.(34%)	1306		
	ν_7 C-O str. $_{ip}$ (74%)	1385	1404 w	1407 w
	ν_8 C-H wag $_{ip}$ (47%)	1043	1063 w	1067 s
	ν_9 Ring breath (66%)	939	965 m	977 vs
	ν_{11} Ring bend (56%)	738	771 w	769 w,sh
	ν_{12} Ring bend (69%)	529	510 vw	
	ν_{13} CCO def. $_{ip}$ (68%)	364		407 w
A_2	ν_{14} C-H wag $_{ip}$ (55%)	577		
	ν_{15} Ring def. (955)	722		757 vvs
	ν_{16} Ring def. (89%)	191		185
B_1	ν_{17} C-H str. $_{op}$ (100%)	2982		3031 w
	ν_{20} Ring str. (67%)	1540	1551 ms	1556 m

	ν_{21} Ring str.(33%)	1442	1448 ms	
	ν_{22} Ring str.(49%)	1281	1318 m	1332 m
	ν_{23} C-H wag $_{ip}$ (76%)	1043		
	ν_{24} O-H wag $_{op}$ (76%)	-		
	ν_{25} C_4-H wag (43%)	929	927 w,br	
	ν_{26} C_1-H wag (42%)	1184	~ 1142 m	1148 m
	ν_{27} C-O str. $_{op}$ (75%)	1241	1236 m	1237 m
	ν_{28} Ring bend (88%)	496	467 br,w	463 vw
	ν_{29} CCO def. $_{op}$ (75%)	521	510 vw	515 w
B_2	ν_{30} C-H wag (58%)	791	832 m	770 w
	ν_{31} C-H wag (25%)	730	713 m	710 vm
	ν_{32} C-H wag $_{ip}$ (74%)	635	618 br,m	627 brw
	ν_{33} Ring def. (94%)	576	546 vm	549 m
	ν_{34} Ring def. (76%)	290		251 m
	ν_{36} Ring def. (79%)	133		154 ms

* Same normal mode descriptions as in resorcinol and its isotopomer are used for easier comparison.
** See footnotes of Table 8 for abbreviations.

4.2.2 Molecular docking analysis

During the past decades resorcinol exhibited a number of medical applications, especially as it is used as a starting material to prodcue derivatives of Active Pharmaceutical Ingredients (API) for treating Alzheimer's disease, sickle cell anemia and alcoholism [22]. However, resorcinol itself has been also used as a topical agent in treating dermatological diseases such as eczema, acne and Hidradenitis Suppurativa (HS). Molecular docking is a useful tool used in structure-based drug design (SBDD) to predict binding affinities of an API with specific protein targets [30] that play a role in the pathology of a disease. Resorcinol possess keratolytic properties and hence is known to target the follicular keratin plug which is the initiation stage of several HS lesions [29]. Therefore, a molecular docking analysis is useful to provide insights on the modes of action of resorcinol in treating HS. The structure of the target protein, keratin-7, was obtained from the protein database bank with PDB ID-4XIF [113], and Ramachandran plot was carried out to validate its structure where target protein should maintain a Ramachandran outlier less than 5% [95]. The Ramachandran plot gave an outlier value of 2.769% which indicated a good quality protein which can be used to accomplish conclusive molecular docking scenarios.

The optimized structures of the three resorcinol rotamers (Scheme 1) were trailed for docking with keratin-7 (Fig. 15). The binding affinities in terms of score values of the generated pose structures of resorcinol after binding with the protein are listed in Table 11. The three conformers of resorcinol showed similar binding affinities towards keratin-7 indicating that the stable mode of action of resorcinol with the target protein is irrelevant of the rotameric form it undergoes. Moreover, the steric interactions were expected to play

the major role in the docking process compared to hydrogen bonding. Due to the small size of the resorcinol molecule, keratin-7 seems to be capable of availing sterically favored regions to accommodate stable protein-ligand binding. Steric interaction is made up of non-polar, polar to non-polar, repulsive interactions, etc. that other than hydrogen bonding interaction [96].

Docking analysis, moreover, showed that while hydrogen bonding is not the most significant factor compared to steric interaction as discussed above, yet it shows an appreciable contribution to the stable protein-ligand long-distance binding. For example, in the case of rotamer **AS**, the computed favorable possibilities included three different hydrogen bonding interactions represented in Fig. 16 and were carefully tracked. Due to their high electronegativity, the two oxygen atoms of resorcinol exhibited a significant role in the biological activity of the ligand towards keratin-7. The molecule of resorcinol acts as both a hydrogen bond donor and acceptor towards ASN 557 giving rise to a stable conventional hydrogen protein-ligand bonding. Non-conventional O···HC interaction between resorcinol and THR 809 with a calculated distance of 2.6 Å was also predicted [114]. On the other hand, a hydrophobic interaction of pi-alkyl type with LYS 898 is well-maintained within an approximity of 4.5 Å. These four interactions account for the binding affinity for **AS** and, with the remarkable facilitation of the steric factor, are responsible for the keratolytic properties of resorcinol with keratin. Other two rotamers also showed similar types of interaction resulting with comparable overall docking scores.

Table 11. Binding affinities of different conformers of resorcinol with Keratin (PDB ID: 4XIF)

Rotamer	Binding Site	HB Score	SI Score	LCP	Final Docking Score
AS	A	-9.53	-27.75	0.00	-37.28
	B	-9.69	-26.99	0.00	-36.68
	C	-7.56	-27.64	0.00	-35.20
	D	-10.00	-27.56	0.00	-37.56
A	A	-9.38	-27.45	0.00	-36.83
	B	-9.60	-27.04	0.00	-36.63
	C	-9.61	-26.96	0.00	-36.57
	D	-10.00	-27.27	0.00	-37.27
S	A	-9.50	-27.85	0.00	-37.34
	B	-9.40	-27.13	0.00	-36.53
	C	-9.99	-26.33	0.00	-36.32
	D	-9.69	-27.83	0.00	-37.52

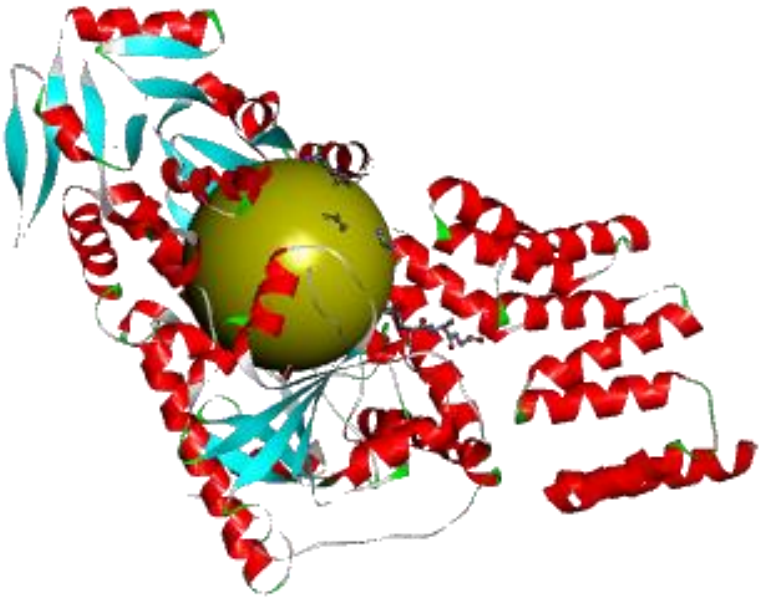

Figure 15. The tertiary structure of keratin-7 (PDB ID -4XIF). The binding site is indicated with a yellow sphere.

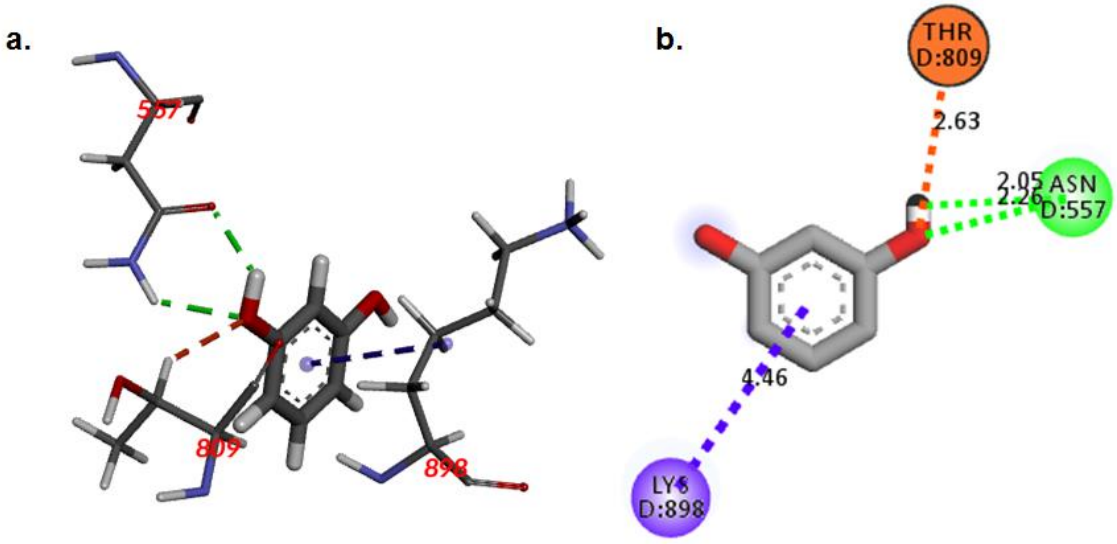

Figure 16. (a) The binding modes, and (b) molecular interactions of AS rotamer with the amino residues of keratin-7 (PDB ID: 4XIF). Interactions labelled as green, red and purple refer to hydrogen-bonding, carbon-hydrogen, and π-alkyl types of interaction, respectively. Bond distances are given in Å.

4.2.3 Conclusion

The B3LYP/6-311++G(d,p) computational method was utilized to optimize the unit cell of the crystal structure of α-resorcinol and to calculate the associated harmonic frequencies helped in understanding some spectroscopic differences in the infrared and Raman spectra between the solid and the gas phases. The potential energy distribution of the normal vibrational modes was done using the VEDA program. The AS rotamer is the most stable and also was the best pose in which the resorcinol molecule bound to the target protein keratin-7(PDB-4XIF) in the molecular docking analysis which gave an insight to the keratolytic property of resorcinol in HS lesions.

4.3 Molecular Docking of other Bioactive compounds

4.3.1 Molecular Docking of MNPE

The validation of the structure of the target protein is an essential step in the drug discovery process [115]. The crystal structure of a human GABA receptor (PDB ID: 4COF) shown in Fig. 10a was done at a resolution of 2.97 Å and was used as the target protein [116]. The target protein contains 5 possible binding sites, namely chains A, B, C, D and E. Each chain is consisted of about five α-helices which are spiral in shape and about 8 β-pleated sheets. Ramachandran plot (Fig. 17b) checked a total number of 1574 residues out of the 1665 amino residues present in the target protein, which is tantamount to about 95% of the total residues. The total number of core regions and outliers are 1546 and 28 respectively, which gave a rise to a percentage outlier of 1.8 %. The Ramachandran plot uses percentage outlier to ascertain the validity of a protein structure. The recommended range for the percentage outlier for a valid protein structure is between 0 to 5 % [95]. Hence, the target protein (PDB ID: 4COF) used for the molecular docking was valid. The five binding sites of the

benzamidine molecule, A, B, C, D and E, complexed with the crystal structure of the target protein (PDB ID: 4COF) were used for docking analysis. Benzamidine is an agonist for the human GABA receptor [116] and hence its binding site was used as a reference for the molecular docking analysis. Table 12 lists the molecular docking results of (4-(3-methoxy-4-nitrophenyl)piperazin-1-yl)ethanone (MNPE) and human GABA receptor. Binding site C which is the reference site for BEN C in the original crystal structure had the highest total docking score value which implies that MNPE exhibits the best binding affinity towards the target protein within this binding site. The total score value is the sum of the Hydrogen Bond (HB) score, the Steric Interaction (SI) score and the ligand penalty conformation. It was also predicted that the ligand in binding cite C has the lowest ligand conformation penalty value (7.910) and the most negative steric interaction score (-59.781) among the different binding sites. Four types of favorable interactions (Fig. 18) between MNPE and the target protein could be established. The favorable interactions between MNPE and the target protein included conventional hydrogen bonding with amino acids THR 202 and GLN 64, π-π stacking and π-alkyl interactions with PHE 200, TYR 62 and TYR 205, and carbon hydrogen bond with ASP 43 and TYR 157 (Fig. 18). The molecular docking analysis involved the generation of five low energy conformational scenarios known as poses. Unlike regular conformations, a pose structure is dependent on the target protein. Each pose was screened against the target protein in each of the five binding sites, A thru E. The binding mode conformation of MNPE in a binding site C have shown the best binding affinity (Fig. 18). During molecular docking analysis, the molecule orientated itself such that there exists an intramolecular hydrogen bonding between one of the hydrogens of the piperazine ring and the oxygen of the carbonyl group. The comparison

between the most stable conformer (B4) and the best binding pose from the molecular docking analysis is depicted in Fig. 19. It was evident that the docked pose and most stable conformer of MNPE were similar with respect to the position of the various functional groups except that the structure of the binding pose is contracted due to the presence of intramolecular hydrogen bonding along with its orientation of the flexible bonds in the molecule. The difference in the structure of the binding pose arises because in molecular docking the molecule would orientate itself such that it best-fit into the binding pocket of the target protein to ensure adequate binding.

Table 12: The docking results of the title compound with the human GABA receptor.

Binding Sites	HB score	SI score	Ligand conformation penalty	Total Score
A	-6.000	-53.167	6.611	-52.556
B	-5.513	-52.730	6.671	-51.572
C	-6.596	-59.781	7.910	-58.468
D	-8.628	-51.792	6.624	-53.795
E	-5.886	-53.699	6.687	-52.898

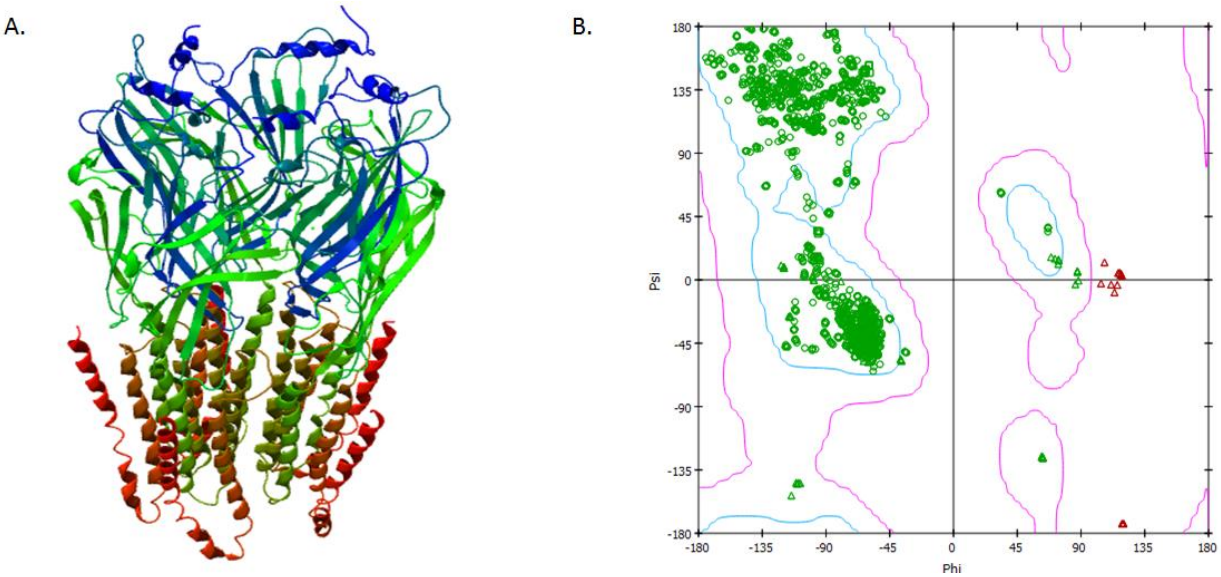

Figure 17. (A) The crystal structure of a human GABA receptor (PDB ID: 4COF). (B) The Ramachandran plot of the crystal structure of a human GABA receptor (PDB ID: 4COF**).**

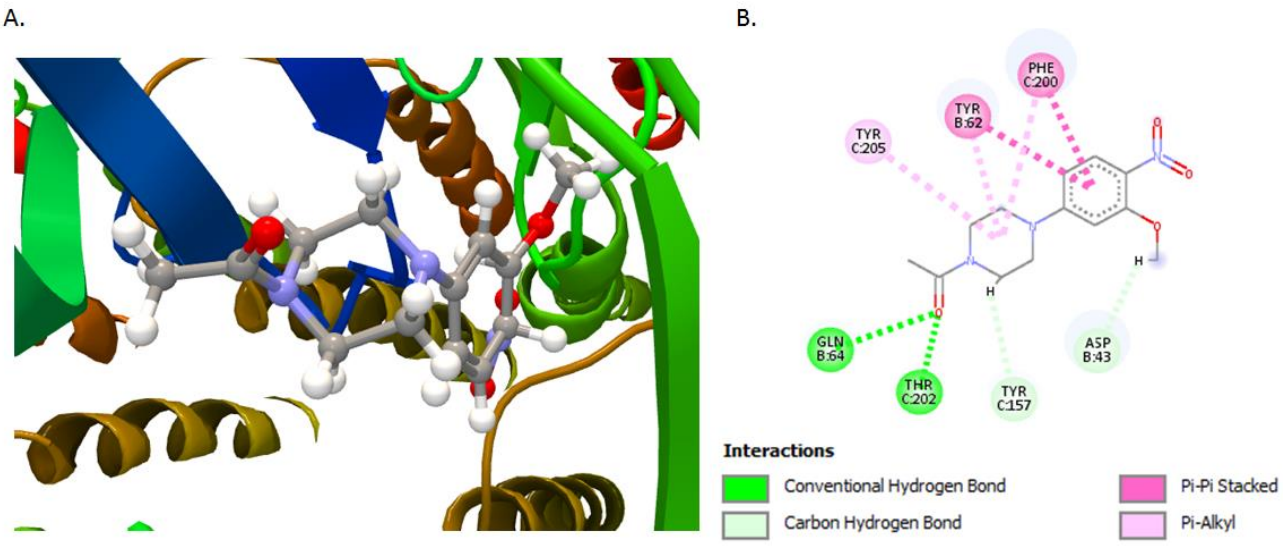

Figure 18. (A) Docked conformation of the title compound in binding site C of GABA (PDB ID: 4COF). (B) The molecular interactions of MNPE and amino acids in binding site *C* of GABA

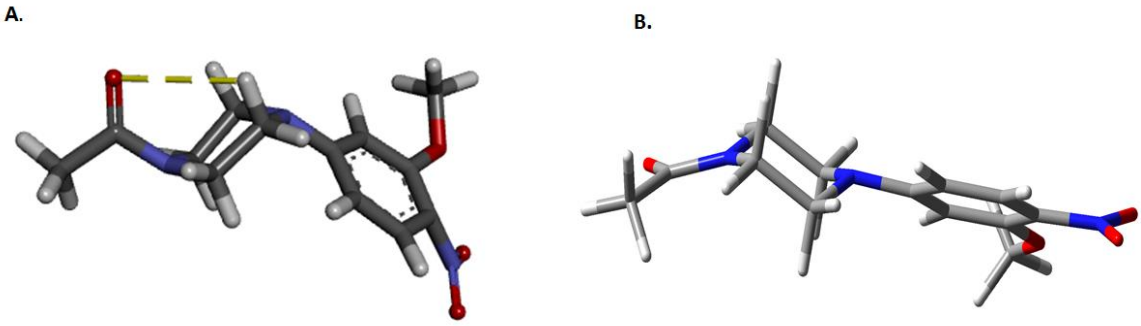

Figure 19. (A) Docked conformation of the title compound in binding site *C* showing the presence of intra-hydrogen bond (shown as yellow color). (B) The most stable conformation, B4 of the title compound

4.3.2 Molecular Docking of Gold Complexes

The inhibition of thyroxine (TrxR) is important as a chemotherapeutic treatment, especially with the use of gold and platinum complexes especially the former which has been noted to be responsible in enzyme activity inhibition [117]. However, selenium has also proved to be useful in cancer treatment[118], [119]. Hence, the choice of docking the synthesized gold(1) complexes which all contain selenium with the target protein, thioredoxin reductase (PDB ID: 3EAN) [120]. The protein was validated using the Ramachandran plot with the Moleman 2 [95] to check for the percentage outlier. For a valid protein, the percentage outlier should be between the range of 0 to 5 % [95]. The target protein proved to be valid by having a percentage outlier of 2.7 %.

Table 13. The docking results of gold(I) complexes (1-5) with human thioredoxin reductase-thioredoxin

Compound	Molecular mass	HBD	HBA	cLogP	Rotatable bonds	Ro5 violation	Docking Score	Distance from Sec 498(Å)
1	735.6	2	4	7.05	8	2	-25.75	6.638
2	763.7	1	4	6.87	9	2	-30.20	6.514
3	777.7	1	4	8.41	10	2	-33.87	6.413
4	763.7	1	4	7.67	8	2	-34.45	2.135
5	791.7	1	4	8.84	10	2	316	7.675

The CLC drug discovery workbench [63] program was used to dock the gold complexes to the TrxR (PDB ID: 3EAN). However, the initial ligands were extracted from the target protein before being docked with the gold complexes. The active site in TrxR has been known to include Sec 498 (selenocysteine) which would lead to the formation of the gold-selenolate specie [121] . Hence this was used as the binding site. The complexes were all minimized using Spartan 16 program [122] before being docked in the binding site. The Discovery studio program [97] was used to observed the binding mode and interactions present in the binding pocket of the docked results. All other amino acid interactions present in the binding mode were discarded except for Sec 498. The bond distance between the gold atom present in each complex and the Selenium atom in the Selenocysteine amino acid (Sec 498) was observed using the GaussView program [92]. Complex 4 had the shortest distance of 2.13 Å (Fig. 4) between the gold and selenium which implied that it had the best potential to form the gold-selenolate specie. This bond distance is in fact shorter than what was observed between Auranofin and selenocysteine [123] which is 5.897Å. All the complex showed negative docking scores except complex 5 which implied that there was no binding affinity between the complex and the target protein (TrxR) since the more negative a docking score, the stronger the binding affinity. Moreover, the docking scores correlated with the bond distances between the gold and selenium atoms such that complex 4 which had the shortest bond distance also had the highest docking score and same applied to complex 5 (Table 13).

All the complexes violated the Lipinski's rule of five, by having a molecular mass and calculated logP (clogP) greater than 500 and 5 respectively. However, this does not deter

them from being used as potential anticancer therapeutics since they can all be optimized into lead compounds[124], [125].

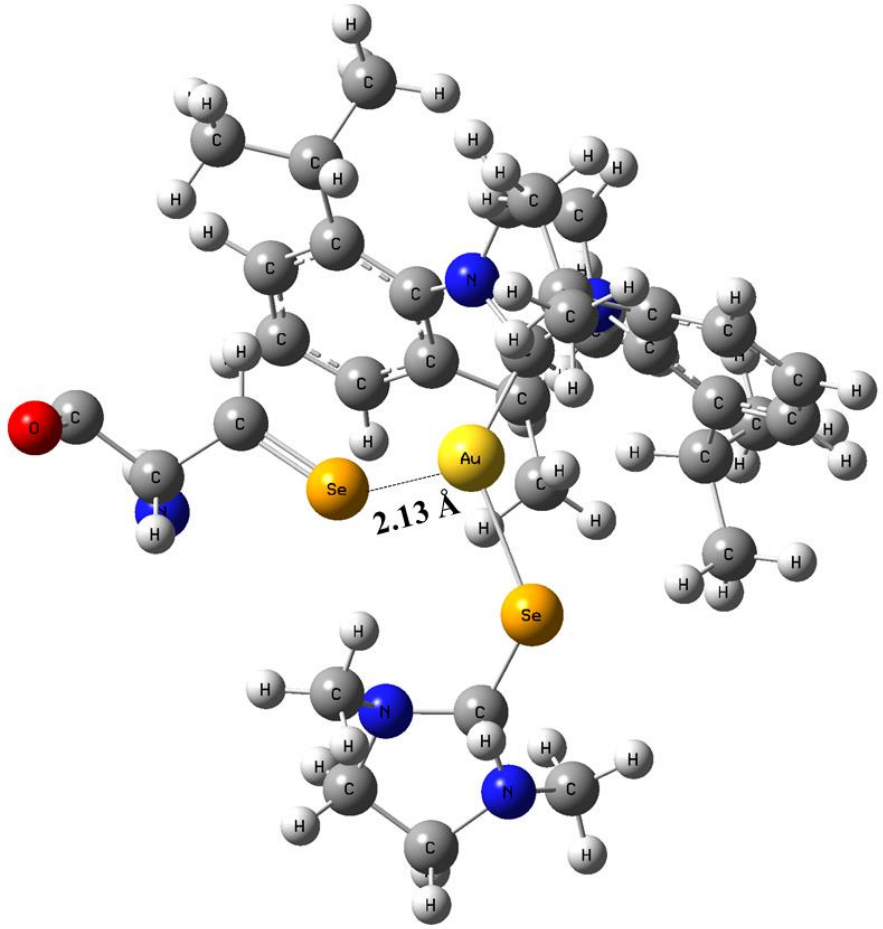

Figure 20. The interaction of complex 4 with Sec 498 in the binding site of TrxR (PDB ID: 3EAN).

4.3.3 Molecular Docking of Ketoconazole

The docking analysis of ketoconazole (KCZ) with the crystal structure of an androgen receptor, PDB ID: 2AX6 [126] was done using CLC drug discovery workbench 3.0 [96]. Ketoconazole is the first non-steroidal compound to bind competitively to a sex steroid globulin. Amongst other antifungal imidazole derivatives such as clotrimazole and fluconazole, ketoconazole is the only one which interacts with the androgen receptor [55]. It acts as an antagonist thereby making it useful in the treatment of androgen-dependent prostate cancer [126]. However, the mode of action of ketoconazole has not really been understood. Molecular docking is an in-silico method that is used in understanding the interactions between ligand in this case, ketoconazole and a target protein (androgen receptor). The validity of the target protein using Ramachandran plot gave an outlier of 0.9%, which falls within the recommended range of 0-5% for a good quality protein [95]. The water molecules were removed before binding the ligand to the receptor and the initial ligand in the crystal structure of the target protein was used as the reference binding site within a radius of 13 Å. The number of iterations was set to 100 to get the best binding mode. After docking the ketoconazole to the androgen receptor, the ligand was optimized to give a docking score of -57.55 which implied a strong binding between the ligand and the receptor since the higher the negative value of a docking score the stronger the binding. The interactions between the ligand and the receptor showed many favorable interactions such as pi-alkyl, pi-cation, hydrogen bond and halogen bond with the amino acids found in the binding site and only two unfavorable interactions with MET 745 and GLN 711 (Fig. 21). The binding mode and molecular interactions between ketoconazole, and the androgen receptor may help understand the former's role in treating prostate cancer.

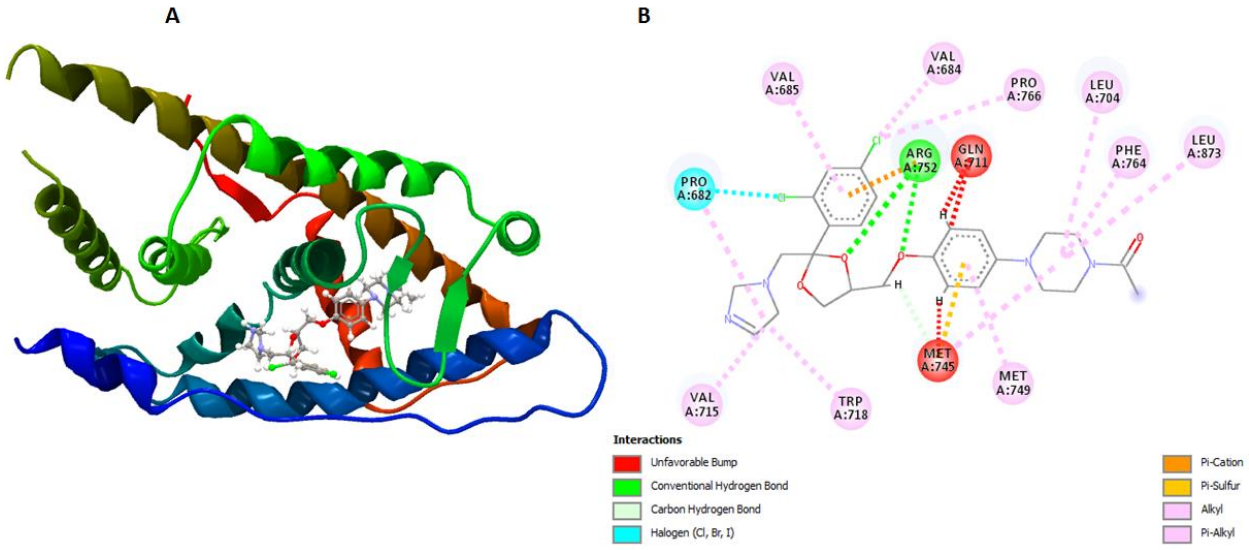

Figure 21. (A) Docked conformation of ketoconazole in the active site of the androgen receptor (PDB: 2AX6). (B) The molecular interactions between ketoconazole and the androgen receptor

4.3.4 Molecular Docking of Methimazole

Methimazole (MTZ) is one of the popular anti-thyroid drugs alongside propyl thiouracil. It acts by inhibiting the enzyme thyroid peroxidase [15] which is responsible for the synthesis of thyroid hormone. Molecular docking helps in understanding the mode of action of methimazole on thyroid peroxidase. The structure of thyroid peroxidase was got from the protein database with PDB ID-1VGE [127]. Ramachandran plot which is a simple and popular way of validating protein structures [128] was used to confirm if the target protein was of good quality before docking it with the ligand (MTZ) using Moleman2 [95]. The percentage Ramachandran outlier for the enzyme thyroid peroxidase is 4.27%. This falls within the accepted range from a good quality protein, which is between 0-5% [95]. The AutoDock Vina [129] tool was used for the docking analysis. The ligand was first minimized before being docked with the target protein. The grid was maximized with a binding center of -22.3540, 26.5288 and 63.0403 for X, Y and Z axes respectively via the PyRx software [130]. The grid covered the whole target protein to ensure that all possible binding sites were considered to get the best binding mode. MTZ had a score value of -4.5 $kcalmol^{-1}$ which showed good binding affinity with the target protein since negative values implies presence of binding affinity while positive values means no binding exist between the ligand and the protein. The Discovery studio visualizer [97] was used to view the possible interactions between MTZ and the target protein, thyroid peroxidase as shown in Fig. 21. The CLC Drug Discovery workbench [96] was used to view the protein-ligand complex between MZM and the target protein. There were three types of favorable bonds present in the protein-ligand interaction of MTZ with thyroid peroxidase. The favorable bonds include the conventional hydrogen bonding to ASP167 and GLU165; a pi-sulfur with HIS 173 and a pi-donor hydrogen bond with THR164.

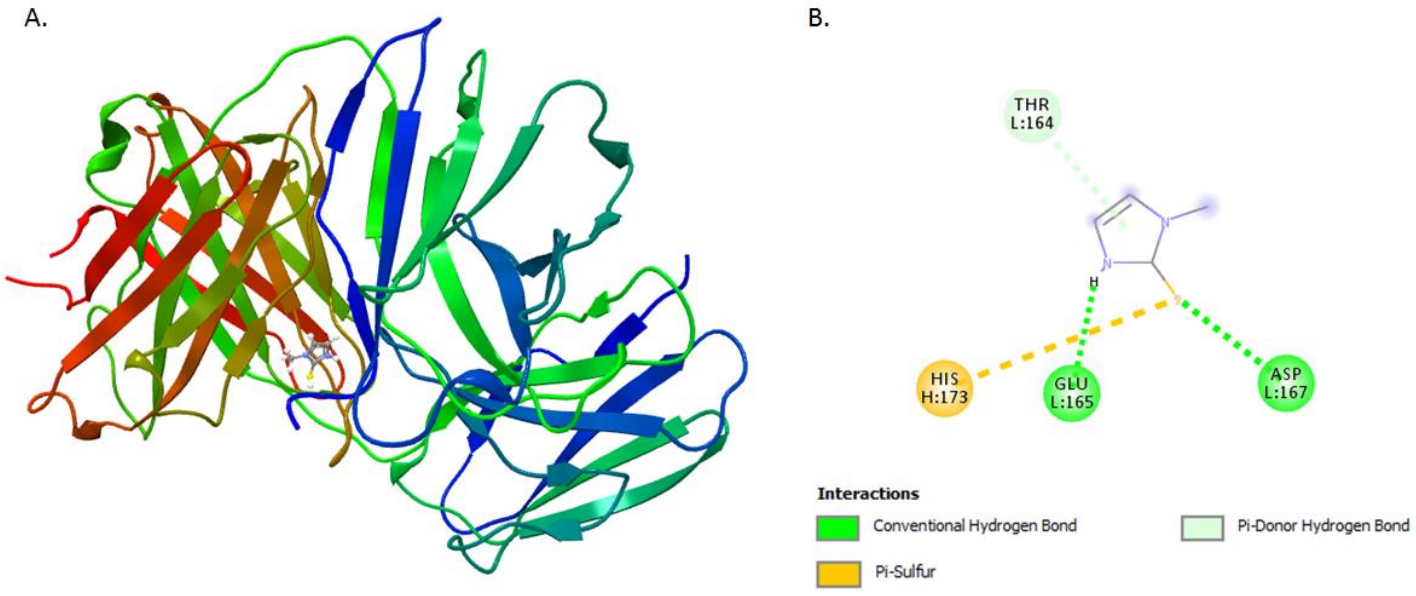

Figure 22. (A) Docked conformation of MZM in thyroid peroxidase (PDB ID: 1VGE). (B) The molecular interactions MZM and amino acids in thyroid peroxidase

4.3.5 Conclusion

The molecular docking analysis of MNPE showed that binding site C had the best binding affinity towards the human $GABA_A$ receptor. For the novel anti cancer seleno-complexes The molecular docking studies indicated that complex 4 had the highest binding affinity (−34.45) and showed the molecular interactions such as, van der Waals, pi-cation and alkyl with the amino group present in the target protein. Complex 4 also had the shortest bond distance between gold atom and Sec 498 of TrxR (2.13 Å), while complex 5 has the highest (7.68 Å). The molecular docking results of the complexes with human thioredoxin reductase enzyme would be helpful to explore their mechanism of action. The molecular interactions between Ketoconazole and the androgen receptor showed many favorable interactions such as pi-alkyl, pi-cation, hydrogen bond and halogen bond with the amino acids found in the binding site and only two unfavorable interactions with MET 745 and GLN 711 while the molecular docking studies of Methimazole with thyroid peroxidase revealed three types of favorable bonds including, the conventional hydrogen bon to ASP167 and GLU165; a pi-sulfur with HIS 173 and a pi-donor hydrogen bond with THR164.

References

[1] H. Song and H.-S. Shin, “The Antifungal Drug Clotrimazole,” *Acta Crystallogr. Sect. C Cryst. Struct. Commun.*, vol. 54, no. 11, pp. 1675–1677, 1998.

[2] I. Kurokawa, F. W. Danby, Q. Ju, X. Wang, L. F. Xiang, L. Xia, W. Chen, I. Nagy, M. Picardo, D. H. Suh, R. Ganceviciene, S. Schagen, F. Tsatsou, and C. C. Zouboulis, “New developments in our understanding of acne pathogenesis and treatment,” *Exp. Dermatol.*, vol. 18, no. 10, pp. 821–832, 2009.

[3] S. Bhambri, J. Q. Del Rosso, and A. Bhambri, “Pathogenesis of acne vulgaris: recent advances.,” *J. Drugs Dermatol.*, vol. 8, no. 7, pp. 615–8, 2009.

[4] I. M. Kapetanovic, “Computer-aided drug discovery and development (CADDD): In silico-chemico-biological approach,” *Chem. Biol. Interact.*, vol. 171, no. 2, pp. 165–176, Jan. 2008.

[5] K. Mayura and B. Amol, “Role of Computational Chemistry in Drug Design,” vol. 5, no. 1, pp. 55–67, 2015.

[6] J. DiMasi, H. Grabowski, and R. Hansen, “Innovation in the pharmaceutical industry: new estimates of R&D costs. Journal of Health Economics,” *J. Health Econ.*, vol. 47, pp. 20–33, 2016.

[7] G. J. Sharman, “Conformation and Stereochemical Analysis of Drug Molecules,” *eMagRes*, vol. 4, pp. 105–116, 2015.

[8] A. Paudel, D. Raijada, and J. Rantanen, “Raman spectroscopy in pharmaceutical product design,” *Adv. Drug Deliv. Rev.*, vol. 89, pp. 3–20, 2015.

[9] W. J. Wishart DS, Knox C, Guo AC, Shrivastava S, Hassanali M, Stothard P, Chang Z and K. C. W. J. Wishart DS Guo AC, Shrivastava S, Hassanali M, Stothard P, Chang Z, “DrugBank: a comprehensive resource for in silico drug discovery and exploration,” *Nucleic Acids Res.*, vol. 84, no. 24, p. 35, 2006.

[10] K. Iwata, H. Yamaguchi, and T. Hiratani, “Mode of Action of Clotrimazole,”

Sabouraudia, pp. 158–166, 1973.

[11] W. L. J. Chaffin, J. L. Lopez-Ribot, M. Casanova, D. Gozalbo, and J. P. Martinez, "Cell Wall and Secreted Proteins of Candida albicans : Identification , Function , and Expression," *Microbiol. Mol. Biol. Rev.*, vol. 62, no. 1, pp. 130–180, 1998.

[12] R. A. Cihlar, R. L., Calderone, *Methods in Molecular Biology, vol.499 - Candida Albicans*. 2009.

[13] G. C. Sauer, "The Fungus among Us The causative agent of the Candidiasis disease is a fungus," *Man. Ski. Dis. 6th Ed.*, pp. 1–5, 1991.

[14] "Vaginal yeast infection," *National Institute of Allergy and Infectious Diseases*, 2015. [Online]. Available: http://www.niaid.nih.gov/topics/vaginalYeast/Pages/Default.aspx. [Accessed: 25-Dec-2015].

[15] D. S. Wishart, C. Knox, A. C. Guo, S. Shrivastava, M. Hassanali, P. Stothard, Z. Chang, and J. Woolsey, "DrugBank: a comprehensive resource for in silico drug discovery and exploration.," *Nucleic Acids Res.*, vol. 34, no. Database issue, pp. D668–D672, 2006.

[16] A. G. Warrilow, J. E. Parker, D. E. Kelly, and S. L. Kelly, "Azole Affinity of Sterol 14 -Demethylase (CYP51) Enzymes from Candida albicans and Homo sapiens," *Antimicrob. Agents Chemother.*, vol. 57, no. 3, pp. 1352–1360, 2013.

[17] F. R. Taylor, R. J. Rodriguez, and L. W. Parks, "Relationship Between Antifungal Activity and Inhibition of Sterol Biosynthesis in Micanazole, Clotrimazole and 15-Azasterol," *Anticancer Res*, vol. 23, no. 4, pp. 515–521, 1983.

[18] E. Bilensoy, M. Abdur Rouf, I. Vural, M. Šen, and A. Atilla Hincal, "Mucoadhesive, thermosensitive, prolonged-release vaginal gel for clotrimazole: β-cyclodextrin complex," *AAPS PharmSciTech*, vol. 7, no. 2, pp. E54–E60, Jun. 2006.

[19] O. Cristini-Robbe, F. Ruyffelaere, F. Dubart, A. Uwimanimpaye, C. Kinowski, R.

Bernard, C. Robbe-Masselot, I. El Yazidi, and S. Turrell, “Local Drug Delivery Strategy for Cancer Treatment: Use of Biocompatible Sol-Gel-Derived Porous Materials,” *New J. Glas. Ceram.*, vol. 3, no. 2, pp. 74–79, 2013.

[20] K. Dhudashia, A. Patel, and C. Patel, “Development and validation of a reversed-phase HPLC method for simultaneous estimation of clotrimazole and beclomethasone dipropionate in lotion and cream dosage form,” *Chronicles Young Sci.*, vol. 4, no. 2, p. 102, 2013.

[21] H. Dressler, *Resorcinol: Its Uses and Derivatives*. New York: Springer Science + Business Media, 1994.

[22] R. B. Durairaj, *Resorcinol-Chemistry Technology & Applications*. 2005.

[23] D. J. Cram, “Cavitands: Organic Hosts with Enforced Cavities,” *Science (80-.).*, vol. 219, no. 4589, 1983.

[24] “NFPA 2010: Standard for Fixed Aerosol Fire-Extinguishing Systems.” 2015.

[25] J. Buckingham, *Dictionary of natural products.* Chapman & Hall, 1994.

[26] V. Ramamurthy and Y. Inoue, *Supramolecular photochemistry : controlling photochemical processes*. Wiley, 2011.

[27] J. D. Kopple, S. G. Massry, and K. Kalantar-Zadeh, *Nutritional Management of Renal Disease.* Elsevier Science, 2013.

[28] K. Drużbicki, E. Mikuli, N. Pałka, S. Zalewski, and M. D. Ossowska-Chruściel, “Polymorphism of Resorcinol Explored by Complementary Vibrational Spectroscopy (FT-RS, THz-TDS, INS) and First-Principles Solid-State Computations (Plane-Wave DFT),” *J. Phys. Chem. B*, vol. 119, no. 4, pp. 1681–1695, 2015.

[29] G. Jemec, J. Revuz, and J. Leyden, *Hidradenitis Suppurativa*. Springer US, 2006.

[30] I. A. Guedes, C. S. de Magalhães, and L. E. Dardenne, “Receptor–ligand molecular docking,” *Biophys. Rev.*, vol. 6, no. 1, pp. 75–87, 2014.

[31] J. R. Naglik, S. J. Challacombe, and B. Hube, “Candida albicans Secreted Aspartyl Proteinases in Virulence and Pathogenesis,” *Microbiol. Mol. Biol. Rev.*, vol. 67, no. 3, pp. 400–428, 2003.

[32] W. L. Chaffin, “Candida albicans Cell Wall Proteins,” *Microbiol. Mol. Biol. Rev.*, vol. 72, no. 3, pp. 495–544, 2008.

[33] M. A. Pfaller, R. N. Jones, S. A. Messer, M. B. Edmond, and R. P. Wenzel, “National surveillance of nosocomial blood stream infection due to Candida albicans: frequency of occurrence and antifungal susceptibility in the SCOPE Program.,” *Diagn. Microbiol. Infect. Dis.*, vol. 31, no. 1, pp. 327–32, May 1998.

[34] J. D. Sobel, “Pathogenesis and epidemiology of vulvovaginal candidiasis.,” *Ann. N. Y. Acad. Sci.*, vol. 544, pp. 547–57, 1988.

[35] W. Li, D. Yu, S. Gao, J. Lin, Z. Chen, and W. Zhao, “Role of Candida Albicans-secreted aspartyl proteinases (Saps) in severe early childhood caries,” *Int. J. Mol. Sci.*, vol. 15, no. 6, pp. 10766–10779, 2014.

[36] A. Tavanti, G. Pardini, D. Campa, P. Davini, A. Lupetti, and S. Senesi, “Differential expression of secretory aspartyl proteinase genes (SAP1-10) in oral Candida albicans isolates with distinct karyotypes,” *J. Clin. Microbiol.*, vol. 42, no. 10, pp. 4726–4734, 2004.

[37] R. de C. Mardegan, M. A. Foglio, R. B. Goncalves, and F. J. Hofling, “Candida albicans proteinases,” *Braz J Oral Sci.*, vol. 5, no. 16, pp. 944–952, 2006.

[38] B. Hube and J. Naglik, “Candida albicans proteinases: resolving the mystery of a gene family,” *Microbiology*, vol. 147, no. 8, pp. 1997–2005, Aug. 2001.

[39] M. Monod, B. Hube, D. Hess, and D. Sanglard, “Differential regulation of SAP8 and SAPS, which encode two new members of the secreted aspartic proteinase family in Candida albicans,” *Microbiology*, vol. 144, no. 10, pp. 2731–2737, Oct. 1998.

[40] B. Hube, M. Monod, D. A. Schofield, A. J. Brown, and N. A. Gow, “Expression of

seven members of the gene family encoding secretory aspartyl proteinases in Candida albicans.," *Mol. Microbiol.*, vol. 14, no. 1, pp. 87–99, Oct. 1994.

[41] S. H. Miyasaki, T. C. White, and N. Agabian, "A fourth secreted aspartyl proteinase gene (SAP4) and a CARE2 repetitive element are located upstream of the SAP1 gene in Candida albicans.," *J. Bacteriol.*, vol. 176, no. 6, pp. 1702–10, Mar. 1994.

[42] T. C. White, S. H. Miyasaki, and N. Agabian, "Three distinct secreted aspartyl proteinases in Candida albicans.," *J. Bacteriol.*, vol. 175, no. 19, pp. 6126–33, Oct. 1993.

[43] M. K. Hostetter, "Adhesins and ligands involved in the interaction of Candida spp. with epithelial and endothelial surfaces.," *Clin. Microbiol. Rev.*, vol. 7, no. 1, pp. 29–42, Jan. 1994.

[44] M. Schaller, H. C. Korting, W. Schäfer, J. Bastert, W. Chen, and B. Hube, "Secreted aspartic proteinase (Sap) activity contributes to tissue damage in a model of human oral candidosis," *Mol. Microbiol.*, vol. 34, no. 1, pp. 169–180, 1999.

[45] B. E. Jackson, K. R. Wilhelmus, and B. Hube, "The role of secreted aspartyl proteinases in Candida albicans keratitis," *Investig. Ophthalmol. Vis. Sci.*, vol. 48, no. 8, pp. 3559–3565, 2007.

[46] M. Schaller, M. Bein, H. C. Korting, S. Baur, G. Hamm, M. Monod, S. Beinhauer, and B. Hube, "The secreted aspartyl proteinases Sap1 and Sap2 cause tissue damage in an in vitro model of vaginal candidiasis based on reconstituted human vaginal epithelium.," *Infect. Immun.*, vol. 71, no. 6, pp. 3227–34, Jun. 2003.

[47] E. Pericolini, E. Gabrielli, M. Amacker, L. Kasper, E. Roselletti, E. Luciano, S. Sabbatini, M. Kaeser, C. Moser, B. Hube, A. Vecchiarelli, and A. Cassone, "Secretory Aspartyl Proteinases Cause Vaginitis and Can Mediate Vaginitis Caused by Candida albicans in Mice.," *MBio*, vol. 6, no. 3, p. e00724, Jun. 2015.

[48] L. A. Braga-Silva and A. L.S. Santos, “Aspartic Protease Inhibitors as Potential Anti-Candida albicans Drugs: Impacts on Fungal Biology, Virulence and Pathogenesis,” *Curr. Med. Chem.*, vol. 18, no. 16, pp. 2401–2419, 2011.

[49] M. Staniszewska, M. Bondaryk, K. Siennicka, J. Piłat, M. Schaller, and W. Kurzątkowski, “Role of aspartic proteinases in Candida albicans virulence. Part II: Expression of SAP1-10 aspartic proteinase during Candida albicans infections in vivo,” *Postep. Mikrobiol.*, vol. 51, no. 2, pp. 137–142, 2012.

[50] B. Didomenico, “Novel antifungal drugs,” *Curr. Opin. Microbiol.*, vol. 2, pp. 509–515, 1999.

[51] J. M. Fostel and P. A. Lartey, “Emerging novel antifungal agents,” *Ther. Focus*, vol. 5, no. 1, pp. 25–32, 2000.

[52] V. Law, C. Knox, Y. Djoumbou, T. Jewison, A. C. Guo, Y. Liu, A. Maciejewski, D. Arndt, M. Wilson, V. Neveu, A. Tang, G. Gabriel, C. Ly, S. Adamjee, Z. T. Dame, B. Han, Y. Zhou, and D. S. Wishart, “DrugBank 4.0: shedding new light on drug metabolism.,” *Nucleic Acids Res.*, vol. 42, no. Database issue, pp. D1091-7, Jan. 2014.

[53] H. J. Smith and Claire Simons, “Proteinase and Peptidase Inhibition-Recent Potential Targets for Drug Development,” *J. Chem. Inf. Model.*, vol. 53, no. 9, pp. 1689–1699, 2013.

[54] M. Borgers, H. Van den Bossche, and M. De Brabander, “The mechanism of action of the new antimycotic ketoconazole.,” *Am. J. Med.*, vol. 74, no. 1B, pp. 2–8, 1983.

[55] C. Eil, “Ketoconazole binds to the human androgen receptor.,” *Horm. Metab. Res.*, vol. 24, no. 8, pp. 367–70, 1992.

[56] M. M. Al-shalalfeh, A. T. Onawole, A. Saleh, and A. A. Al-saadi, “Spherical silver nanoparticles as substrates in surface-enhanced Raman spectroscopy for enhanced characterization of ketoconazole,” *Mater. Sci. Eng. C*, vol. 76, pp. 356–364, 2017.

[57] L. L. Patton, A. J. Bonito, D. A. Shugars, and C. Hill, “A systematic review of the effectiveness of antifungal drugs for the prevention and treatment of oropharyngeal candidiasis in HIV-positive patients,” *Oral Surg Oral Med Oral Pathol Oral Radiol Endod*, vol. 92, pp. 170–179, 2001.

[58] P. R. Sawyer, R. N. Brogden, R. M. Pinder, T. M. Speight, and C. S. Avery, “Clotrimazole : A Review of its Antifungal Activity and Therapeutic Efficacy,” *Drugs*, vol. 9, pp. 424–447, 1975.

[59] C. A. Lipinski, “Lead- and drug-like compounds: The rule-of-five revolution,” *Drug Discov. Today Technol.*, vol. 1, no. 4, pp. 337–341, 2004.

[60] C. A. Lipinski, “Drug-like properties and the causes of poor solubility and poor permeability,” *J. Pharmacol. Toxicol. Methods*, vol. 44, no. 1, pp. 235–249, 2000.

[61] J. H. Rex, T. J. Walsh, J. D. Sobel, S. G. Filler, P. G. Pappas, W. E. Dismukes, and J. E. Edwards, “Practice guidelines for the treatment of candidiasis,” *Clin. Infect. Dis.*, vol. 38, no. 4, pp. 161–189, 2004.

[62] P. G. Pappas, C. A. Kauffman, D. Andes, D. K. Benjamin, Jr., T. F. Calandra, J. E. Edwards, Jr., S. G. Filler, J. F. Fisher, B. Kullberg, L. Ostrosky- Zeichner, A. C. Reboli, J. H. Rex, T. J. Walsh, and J. D. Sobel, “Clinical Practice Guidelines for the Management of Candidiasis: 2009 Update by the Infectious Diseases Society of America,” *Clin. Infect. Dis.*, vol. 48, no. 5, pp. 503–535, 2009.

[63] I. B. Obot, N. O. Obi-Egbedi, and S. A. Umoren, “Experimental and theoretical investigation of clotrimazole as corrosion inhibitor for aluminium in hydrochloric acid and effect of iodide ion addition,” *Der Pharma Chem.*, vol. 1, no. 1, pp. 151–166, 2009.

[64] T. A. Saleh, M. M. Al-shalalfeh, A. T. Onawole, and A. A. Al-saadi, “Ultra-trace detection of methimazole by surface-enhanced Raman spectroscopy using gold substrate,” *Vib. Spectrosc.*, vol. 90, pp. 96–103, 2017.

[65] T. A. Saleh, M. M. Al-Shalalfeh, and A. A. Al-Saadi, “Graphene Dendrimer-

stabilized silver nanoparticles for detection of methimazole using Surface-enhanced Raman scattering with computational assignment," *Sci. Rep.*, vol. 6, no. May, p. 32185, 2016.

[66] E. Rodríguez, A. Encinas, F. J. Masa, and F. J. Beltrán, "Influence of resorcinol chemical oxidation on the removal of resulting organic carbon by activated carbon adsorption," *Chemosphere*, vol. 70, pp. 1366–1374, 2008.

[67] J. Z. Zhang and C. J. Fischer, "A simplified resorcinol method for direct spectrophotometric determination of nitrate in seawater," *Mar. Chem.*, vol. 99, pp. 220–226, 2006.

[68] A. Husain, M. Maaz, K. A. Ansari, A. Ahmad, and M. Rashid, "Synthesis and microbiological evaluation of mannich bases derived from 4,6-diacetylresorcinol," vol. 3, no. 5, pp. 18–20, 2010.

[69] J. M. Robertson, "The Structure of Resorcinol A Quantitative X-Ray Investigation," *Proc. R. Soc. A Math. Phys. Eng. Sci.*, vol. 157, no. 890, pp. 79–99, 1936.

[70] J. M. Robertson and a. R. Ubbelohde, "A New Form of Resorcinol. I. Structure Determination by X-Rays," *Proc. R. Soc. A Math. Phys. Eng. Sci.*, vol. 167, no. 928, pp. 122–135, 1938.

[71] Y. Ebisuzaki, L. H. Askari, a. M. Bryan, and M. F. Nicol, "Phase transitions in resorcinal," *J. Chem. Phys.*, vol. 87, p. 6659, 1987.

[72] T. Dunn, "Free-Jet Spectra and structure of O-, m-, and p-Dihydroxybenzenes," *Chem. Phys. Lett.*, vol. 121, pp. 453–457, 1985.

[73] M. Gerhards, W. Perl, and K. Kleinermanns, "Rotamers and vibrations of resorcinol obtained by spectral hole burning," *Chem. Phys. Lett.*, vol. 240, no. July, pp. 506–512, 1995.

[74] S. Melandri, G. Maccaferri, W. Caminati, and P. G. Favero, "Conformational equilibrium in resorcinol by means of the free-jet absorption millimeter wave

spectrum," *Chem. Phys. Lett.*, vol. 256, no. 4–5, pp. 513–517, Jul. 1996.

[75] G. Myszkiewicz, W. L. Meerts, C. Ratzer, and M. Schmitt, "Structure determination of resorcinol rotamers by high-resolution UV spectroscopy," *ChemPhysChem*, vol. 6, pp. 2129–2136, 2005.

[76] M. Gerhards, M. Schiwek, C. Unterberg, and K. Kleinermanns, "OH stretching vibrations in aromatic cations: IR/PIRI spectroscopy," *Chem. Phys. Lett.*, vol. 297, no. December, pp. 515–522, 1998.

[77] G. M. Day, S. L. Price, and M. Leslie, "Elastic Constant Calculations for Molecular Organic Crystals," *Cryst. Growth Des.*, vol. 1, no. 1, pp. 13–27, 2000.

[78] P. Claudio and T.-K. Ha, "A theoretical study of conformations and rotational barriers in Dihydroxybenzenes," vol. 204, pp. 337–351, 1990.

[79] Z. Berkovitch-Yellin, "Toward an ab Initio Derivation of Crystal Morphology," *J Am Chem Soc*, vol. 107, no. 14, pp. 8239–8253, 1985.

[80] J. Chatchawalsaisin, J. Kendrick, S. C. Tuble, and Jamshed Anwar., "An Optimized force field for crystalline phases of resorcinol," *CrystEngComm*, 2008.

[81] D. Penot, Mathieu, and J. Paul, "The Raman Spectra of Alhpa and Beta Resorcinols," pp. 2–3, 1955.

[82] A. Hidalgo and C. Otero, "Spectres d ' absorption ~~ aro ~ ge du ph6nol et des diphbnols," vol. 16, no. 1943, 1960.

[83] J. H. S. Green, "Vibrational spectra of benzene derivatives - VI. p-disubstituted compounds," *Spectrochim. Acta*, vol. 26A, no. 1968, pp. 1503–1513, 1970.

[84] S. E. Blanco, M. C. Almandoz, and F. H. Ferretti, "Determination of the overlapping pKa values of resorcinol using UV-visible spectroscopy and DFT methods," *Spectrochim. Acta - Part A Mol. Biomol. Spectrosc.*, vol. 61, pp. 93–102, 2005.

[85] R. Rudyk, M. a. . Molina, M. . Gómez, S. . Blanco, and F. . Ferretti, "Solvent

effects on the structure and dipole moment of resorcinol," *J. Mol. Struct. THEOCHEM*, vol. 674, no. 1–3, pp. 7–14, Apr. 2004.

[86] W. Wilson, "The Vapor Phase infrared spectra of hydroquinone, pyrocatechol, and resorcinol," 1974.

[87] P. Imhof, R. Brause, and K. Kleinermanns, "Determination of Ground State Vibrational Frequencies of Jet-Cooled Resorcinol by Means of Dispersed Fluorescence Spectroscopy and ab Initio Calculations," *J. Mol. Spectrosc.*, vol. 211, no. 1, pp. 65–70, Jan. 2002.

[88] G. N. R. Tripathi, "Crystal spectra and vibrational assignments in α-resorcinol," *J. Chem. Phys.*, vol. 74, p. 250, 1981.

[89] K. Hattori, S. I. Ishiuchi, D. L. Howard, H. G. Kjaergaard, M. Fujii, D. L. Howard, and H. G. Kjaergaard, "Vibrational OH-stretching overtone spectroscopy of jet-cooled resorcinol and hydroquinone rotamers," *J. Phys. Chem. A*, vol. 111, pp. 6028–6033, 2007.

[90] G. E. S. M. J. Frisch, G. W. Trucks, H. B. Schlegel, B. M. M. A. Robb, J. R. Cheeseman, G. Scalmani, V. Barone, H. P. H. G. A. Petersson, H. Nakatsuji, M. Caricato, X. Li, M. H. A. F. Izmaylov, J. Bloino, G. Zheng, J. L. Sonnenberg, T. N. M. Ehara, K. Toyota, R. Fukuda, J. Hasegawa, M. Ishida, J. Y. Honda, O. Kitao, H. Nakai, T. Vreven, J. A. Montgomery, E. B. J. E. Peralta, F. Ogliaro, M. Bearpark, J. J. Heyd, J. N. K. N. Kudin, V. N. Staroverov, T. Keith, R. Kobayashi, J. T. K. Raghavachari, A. Rendell, J. C. Burant, S. S. Iyengar, J. B. C. M. Cossi, N. Rega, J. M. Millam, M. Klene, J. E. Knox, R. E. S. V. Bakken, C. Adamo, J. Jaramillo, R. Gomperts, J. W. O. O. Yazyev, A. J. Austin, R. Cammi, C. Pomelli, G. A. V. R. L. Martin, K. Morokuma, V. G. Zakrzewski, A. D. D. P. Salvador, J. J. Dannenberg, S. Dapprich, J. C. O. Farkas, J. B. Foresman, J. V. Ortiz, and and D. J. Fox, "Gaussian 09, Revision D.01," *Gaussian, Inc. Wallingford CT*. 2013.

[91] M. H. Jamróz, "Vibrational energy distribution analysis (VEDA): Scopes and limitations," *Spectrochim. Acta - Part A Mol. Biomol. Spectrosc.*, vol. 114, pp.

220–230, 2013.

[92] T. K. R. Dennington J. Millam, R. Dennington, T. Keith, and J. Millam, "GaussView," vol. 131 TS-, no. 37. Semichem Inc, Shawnee Mission KS, 2009.

[93] A. A. Al-Saadi and J. Laane, "Ab initio and DFT calculations for the structure and vibrational spectra of cyclopentene and its isotopomers," *J. Mol. Struct.*, vol. 830, no. 1–3, pp. 46–57, 2007.

[94] H. M. Berman, J. D. Westbrook, Z. Feng, G. L. Gilliland, T. N. Bhat, H. Weissig, I. N. Shindyalov, P. E. Bourne, T. Battistuz, T. N. Bhat, W. F. Bluhm, E. Philip, K. Burkhardt, Z. Feng, G. L. Gilliland, L. Iype, S. Jain, P. Fagan, J. Marvin, D. Padilla, V. Ravichandran, N. Thanki, H. Weissig, and J. D. Westbrook, "The Protein Data Bank.," *Nucleic Acids Res.*, vol. 28, no. 1, pp. 235–242, 2000.

[95] G. J. Kleywegt and T. A. Jones, "Phi/Psi-chology: Ramachandran revisited," *Structure*, vol. 4, no. 12, pp. 1395–1400, 1996.

[96] T. Knudsen, Bjarne Knudsen, "CLC Drug Discovery Workbench." pp. 1–367, 2016.

[97] D. S. BIOVIA, "Discovery Studio Modeling Environment." Dassault Systèmes, San Diego, 2015.

[98] G. Roussy and F. Michel, "Spectres de rotation de la molécule de chlorobenzéne," *J. Mol. Struct.*, vol. 30, no. 2, pp. 399–407, Feb. 1976.

[99] R. D. Johnson, "NIST Computational Chemistry Comparison and Benchmark Database." [Online]. Available: http://cccbdb.nist.gov/. [Accessed: 28-May-2017].

[100] Kuchitsu, *Landolt-Bornstein: Group II: Atomic and Molecular Physics Volume 15: Structure Data of Free Polyatomic Molecules*. Berlin: Springer-Verlag, 1987.

[101] R. Ramasamy, "Vibrational spectroscopic studies of Imidazole," *Armen. J. Phys.*, vol. 8, no. 1, pp. 51–55, 2015.

[102] R. Ramasamy and B. Dhanaraj, "Vibrational Spectroscopic Studies of Toluene," *J.*

Int. Acad. Res. Multidiscip., vol. 2, no. 4, pp. 234–240, 2014.

[103] Z. El Adnani, M. Mcharfi, M. Sfaira, M. Benzakour, A. T. Benjelloun, and M. Ebn Touhami, "DFT theoretical study of 7-R-3methylquinoxalin-2(1H)-thiones (RH; CH3; Cl) as corrosion inhibitors in hydrochloric acid," *Corros. Sci.*, vol. 68, pp. 223–230, 2013.

[104] S. B. Ade, N. V. Shitole, and S. M. Lonkar, "Antifungal drug's used as metal corrosion inhibitor in various acid medium," *Int. J. ChemTech Res.*, vol. 6, no. 7, pp. 3642–3650, 2014.

[105] B. Hube, "Candida albicans secreted aspartyl proteinases.," *Curr. Top. Med. Mycol.*, vol. 7, no. 1, pp. 55–69, Dec. 1996.

[106] F. M. Klis, G. J. Sosinska, P. W. J. De Groot, and S. Brul, "Covalently linked cell wall proteins of Candida albicans and their role in fitness and virulence," *FEMS Yeast Res.*, vol. 9, no. 7, pp. 1013–1028, 2009.

[107] P. Manivannan and G. Muralitharan, "Molecular modeling of abc transporter system — permease proteins from Microcoleus chthonoplastes PCC 7420 for effective binding against secreted aspartyl proteinases in Candida albicans — A therapeutic intervention," *Interdiscip. Sci. Comput. Life Sci.*, vol. 6, no. 1, pp. 63–70, 2014.

[108] S. M. Cutfield, E. J. Dodson, B. F. Anderson, P. C. Moody, C. J. Marshall, P. A. Sullivan, and J. F. Cutfield, "The crystal structure of a major secreted aspartic proteinase from Candida albicans in complexes with two inhibitors.," *Structure*, vol. 3, no. 11, pp. 1261–71, Dec. 1995.

[109] T. Lengauer and M. Rarey, "Computational methods for biomolecular docking," *Curr. Opin. Struct. Biol.*, vol. 6, no. 3, pp. 402–406, 1996.

[110] J. C. Sundaramurthi, S. Kumar, K. Silambuchelvi, and L. E. Hanna, "Molecular docking of azole drugs and their analogs on CYP121 of Mycobacterium tuberculosis.," *Bioinformation*, vol. 7, no. 3, pp. 130–3, 2011.

[111] G. J. Kleywegt and T. A. Jones, “Phi/Psi-chology,” *Structure*, vol. 4, no. 12, pp. 1395–1400, 1996.

[112] Q. Zhu, A. G. Shtukenberg, D. J. Carter, T. Yu, J. Yang, M. Chen, P. Raiteri, A. R. Oganov, B. Pokroy, I. Polishchuk, P. J. Bygrave, G. M. Day, A. L. Rohl, M. E. Tuckerman, and B. Kahr, “Resorcinol Crystallization from the Melt: A New Ambient Phase and New ‘ Riddles ,’” *J Am Chem Soc*, vol. 138, pp. 4881–4889, 2016.

[113] S. Pathak, J. Alonso, M. Schimpl, K. Rafie, D. E. Blair, V. S. Borodkin, A. W. Schüttelkopf, O. Albarbarawi, and D. M. F. van Aalten, “The active site of O-GlcNAc transferase imposes constraints on substrate sequence.,” *Nat. Struct. Mol. Biol.*, vol. 22, no. 9, pp. 744–750, Aug. 2015.

[114] S. Horowitz and R. C. Trievel, “Carbon-oxygen hydrogen bonding in biological structure and function.,” *J. Biol. Chem.*, vol. 287, no. 50, pp. 41576–82, Dec. 2012.

[115] M. E. Bunnage, A. M. Gilbert, L. H. Jones, and E. C. Hett, “Know your target, know your molecule,” *Nat. Chem. Biol.*, vol. 11, no. 6, pp. 368–372, 2015.

[116] P. S. Miller and A. R. Aricescu, “Crystal structure of a human GABAA receptor,” *Nature*, vol. 512, no. 7514, pp. 270–275, Jun. 2014.

[117] S. Urig, K. Fritz-Wolf, R. Réau, C. Herold-Mende, K. Tóth, E. Davioud-Charvet, and K. Becker, “Undressing of Phosphine Gold(I) Complexes as Irreversible Inhibitors of Human Disulfide Reductases,” *Angew. Chemie Int. Ed.*, vol. 45, no. 12, pp. 1881–1886, Mar. 2006.

[118] L. H. Duntas, “The Role of Selenium in Thyroid Autoimmunity and Cancer,” *Thyroid*, vol. 16, no. 5, pp. 455–460, May 2006.

[119] B. M. Selenius M, Rundlöf AK, Olm E, Fernandes AP, “Selenium and the selenoprotein thioredoxin reductase in the prevention, treatment and diagnostics of cancer.,” *Antioxid. Redox. Signal.*, vol. 12, no. 7, pp. 867–80, 2010.

[120] Q. Cheng, T. Sandalova, Y. Lindqvist, and E. S. J. Arnér, “Crystal structure and

catalysis of the selenoprotein thioredoxin reductase 1.," *J. Biol. Chem.*, vol. 284, no. 6, pp. 3998–4008, Feb. 2009.

[121] P. K. Bhabak, J. B. Bhuyan, and G. Mugesh, "Bioinorganic and medicinal chemistry: aspects of gold(I)-protein complexes," *Dalt. Trans.*, vol. 40, pp. 2099–2111, 2011.

[122] J. Y. Y. Shao, L. Fusti-Molnar, Y. Jung, J. Kussmann, C. Ochsenfeld, S.T. Brown, A.T.B. Gilbert, L.V. Slipchenko, S.V. Levchenko, D.P. O'Neill, R.A. DiStasio Jr., R.C. Lochan, T. Wang, G.J.O. Beran, N.A. Besley, J.M. Herbert, C.Y. Lin, T. Van Voorhis, S.H. Chie, "Spartan'10 build 1.0.1." Wavefunction Inc., Irvine CA, p. Irvine CA, 2011.

[123] T. Shoeib, D. W. Atkinson, and B. L. Sharp, "Structural analysis of the anti-arthritic drug Auranofin: Its complexes with cysteine, selenocysteine and their fragmentation products," *Inorganica Chim. Acta*, vol. 363, no. 1, pp. 184–192, 2010.

[124] A. T. Maynard, C. D. Roberts, M. Drive, N. Carolina, and U. States, "Quantifying, Visualizing, and Monitoring Lead Optimization," 2016.

[125] F. Z. Dorwald, *Lead Optimisation for Medicinal Chemists*. 2012.

[126] C. Bohl, D. Miller, J. Chen, C. Bell, and J. Dalton, "Structural Basis for Accommodation of Nonsteroidal Ligands in the Androgen Receptor," *J. Biol. Chem.*, vol. 280, no. 45, pp. 37747–37754, 2005.

[127] S. Chacko, E. A. Padlan, S. Portolano, S. M. McLachlan, and B. Rapoport, "Structural Studies of Human Autoantibodies: CRYSTAL STRUCTURE OF A THYROID PEROXIDASE AUTOANTIBODY FAB," *J. Biol. Chem.*, vol. 271, no. 21, pp. 12191–12198, May 1996.

[128] S. C. Lovell, I. W. Davis, W. B. Adrendall, P. I. W. de Bakker, J. M. Word, M. G. Prisant, J. S. Richardson, and D. C. Richardson, "Structure validation by C alpha geometry: phi,psi and C beta deviation," *Proteins-Structure Funct. Genet.*, vol. 50,

no. August 2002, pp. 437–450, 2003.

[129] O. Trott and A. Olson, “AutoDock Vina: improving the speed and accuracy of docking with a new scoring function, efficient optimization and multithreading,” *J. Comput. Chem.*, vol. 31, no. 2, pp. 455–461, 2010.

[130] S. Dallakyan and A. J. Olson, “Small-Molecule Library Screening by Docking with PyRx,” 2015, pp. 243–250.

Vitae

Name :Abdulmujeeb Toluwase Onawole

Nationality :Nigerian

Date of Birth :5/14/1989

Email :atonawole@gmail.com

Address :10, Aruba, Sabo, Sagamu, Ogun state, Nigeria

Academic Background :B. Tech (Pure and Applied Chemistry), Ladoke Akintola University of Technology, Ogbomoso, Nigeria (2011); MSc. (Chemistry), King Fahd University of Petroleum and Minerals, Dhahran, Saudi Arabia (2017)

Publications:

[1] **A. T. Onawole**, A. F. Al-Ahmadi, Y. S. Mary, C. Y. Panicker, N. Ullah, S. Armaković, S. J. Armaković, C. V. Alsenoy, and A. A. Al-Saadi, "Conformational, vibrational and DFT studies of a newly synthesized arylpiperazine-based drug and evaluation of its reactivity towards the human GABA receptor," J. Mol. Struct., vol. 1147, pp. 266–280, 2017.

[2] A. A. A. Seliman, M. Altaf, **A. T. Onawole**, S. Ahmad, M. Y. Ahmed, A. A. Al-Saadi, S. Altuwaijri, G. Bhatia, J. Singh, and A. A. Isab, "Synthesis, X-ray structures and anticancer activity of gold(I)-carbene complexes with selenones as co-ligands and their molecular docking studies with thioredoxin reductase," J. Organomet. Chem., vol. 848, pp. 175–183, 2017.

[3] T. A. Saleh, M. M. Al-shalalfeh, **A. T. Onawole**, and A. A. Al-saadi, "Ultra-trace detection of methimazole by surface-enhanced Raman spectroscopy using gold substrate," Vib. Spectrosc., vol. 90, pp. 96–103, 2017.

[4] **A. T. Onawole**, K. O. Sulaiman, R. O. Adegoke, and T. U. Kolapo, "Identification of potential inhibitors against the Zika virus using consensus scoring," J. Mol. Graph. Model., vol. 73, pp. 54–61, 2017.

[5] M. M. Al-shalalfeh, **A. T. Onawole**, A. Saleh, and A. A. Al-saadi, "Spherical silver nanoparticles as substrates in surface-enhanced Raman spectroscopy for enhanced characterization of ketoconazole," Mater. Sci. Eng. C, vol. 76, pp. 356–364, 2017.

[6] K. O. Sulaiman and **A. T. Onawole**, "Quantum chemical evaluation of the corrosion inhibition of novel aromatic hydrazide derivatives on mild steel in hydrochloric acid," Comput. Theor. Chem., vol. 1093, pp. 73–80, 2016.

Conference Proceedings:

[1] **A. T. Onawole** and A. A. Al-Saadi, "Computational study of the conformations and molecular docking of the anti-fungal drug clotrimazole in aiding drug delivery via nanostructured lipid carriers," Poster session presented at: Kuwait International Nanotechnology Conference & Exhibitions, 2016 Feb 9-11; Regency Hotel, State of Kuwait.